Aust. J. Phys., 1987, **40**, 239–81

Near-threshold Rotational and Vibrational Excitation of H_2 by Electron Impact: Theory and Experiment

M. A. Morrison,[A] *R. W. Crompton,*[B] *Bidhan C. Saha*[A] *and Z. Lj. Petrović*[B,C]

[A] Department of Physics and Astronomy, University of Oklahoma, Norman, OK 73069, U.S.A.
[B] Research School of Physical Sciences, Australian National University, G.P.O. Box 4, Canberra, A.C.T. 2601.
[C] Permanent address: Institute of Physics, University of Belgrade, P.O. Box 57, 11001 Belgrade, S.R. Serbia, Yugoslavia.

Table of Contents

0004-9506/87/030239$02.00

Abstract

A joint experimental–theoretical attack on low-energy e–H_2 scattering is described. The cross sections calculated from a highly converged numerical solution of the nonrelativistic Schrödinger equation, using a parameter-free interaction potential, are first compared with results from swarm experiments, and are later used to improve the accuracy of the swarm analysis at energies above the first vibrational threshold. To provide further perspective, the theoretical results are compared with a variety of other experimental data. The theoretical results for the momentum-transfer and rotational-excitation cross sections are in excellent agreement with the results from swarm experiments, but there is an unresolved and significant difference in the threshold behaviour of the vibrational-excitation cross sections. Both the theoretical and experimental approaches are subjected to close scrutiny in an attempt to uncover possible sources of error that could explain this difference. The failure to locate likely sources points to the need for further independent theoretical and experimental work to resolve a problem that has serious implications.

1. Introduction

In spite of progress by experimentalists and theorists during the past 20 years, the present state of knowledge of cross sections for low-energy electron–molecule scattering is fragmentary and inadequate (see, for example, reviews by Lane 1980 and Trajmar *et al.* 1983). Experimentalists have applied crossed-beam techniques and (for very low scattering energies) swarm techniques to electron–molecule collisions, and theorists have implemented close-coupling and L^2-variational methods using a variety of model potentials. Nevertheless, significant uncertainties persist about the actual values of elastic and inelastic cross sections for even very simple systems.

The nature and extent of these uncertainties can be seen in a comparative survey of low-energy cross sections for 'small-molecule' systems, such as H_2, N_2, and CO_2. For example, substantial disagreements pervade the experimental and theoretical literature for near-threshold vibrational excitation of these molecules (Morrison 1987). Moreover, many recent theoretical predictions, such as cross sections for rotational excitation of CO_2 (Morrison and Lane 1979), cannot be compared with experimental data because of the lack of such data. Finally, many important collision processes, such as vibrational excitation of CO_2 and inelastic e–O_2 scattering, simply have not been adequately investigated, either experimentally or theoretically (see, for example, Haddad and Elford 1979).

The principal reason for this state of affairs is the nature of the collision system. For example, two characteristics peculiar to molecular targets plague theorists: the non-spherical character of the target probability density, and the plethora of closely-spaced rotational and vibrational energy levels of even the simplest molecule. These features prevent a rigorous, *ab initio* solution of the electron–molecule Schrödinger equation, even with state-of-the-art computers, for all but the simplest system. Similar difficulties bedevil the experimentalist studying low-energy electron–molecule scattering. For example, the dense mesh of target energy levels requires very high energy resolution in crossed-beam experiments so that scattering processes with small threshold energies can be identified (Jung *et al.* 1982). The analysis of data from swarm experiments, on the other hand, is enormously complicated by the lack of uniqueness caused by the large number of channels that are open even at very low electron energies (Crompton 1983).

This paper is a report of results from a five-year joint experimental–theoretical assault on low-energy electron–molecule scattering. In this program, experimental cross sections are obtained from measured transport data—drift velocities and diffusion coefficients—using an analysis based on the Boltzmann equation (see Section 2).

Theoretical cross sections are obtained from numerical solution of the nonrelativistic Schrödinger equation, using a parameter-free (but approximate) interaction potential (see Section 5).

The objectives of this program are three-fold:

[1] to calculate accurate differential, integral and momentum-transfer cross sections for elastic collisions and ro–vibrational excitations;

[2] to test approximate scattering theories and model potentials by using theoretical cross section data in the transport analysis;

[3] to refine the transport analysis and thereby obtain a more accurate vibrational-excitation cross section by using the most accurate available theoretical rotational-excitation cross sections above the vibrational threshold, by accounting for rotational inelasticity in vibrational excitation, and by applying, if necessary, more rigorous transport theory than has heretofore been used.

An important and, we believe, unique feature of this program is that, although research by the experimental and theoretical groups was performed independently, the two groups have interacted closely and extensively in their subsequent study of the results. For example, we have used transport analysis to test the accuracy of theoretical cross sections for momentum-transfer and ro–vibrational excitation. In this investigation, theoretical cross sections are fed through the Boltzmann equation, which yields transport data. Comparison of the resulting 'theoretical' transport coefficients with measured values provides a unique assessment of the accuracy of approximations used in the theoretical formulation. In return, the theoretical program can provide cross sections for use in subsequent Boltzmann analysis at higher energies, where many channels are open. At these energies, such input is vital because of the aforementioned lack of uniqueness in the transport analysis. A detailed example of this approach appears in Section 4.

In Section 6 we compare theoretical and experimental cross sections, the latter drawn from prior beam experiments and from the present swarm research. Although experiment and theory agree for several scattering processes, a surprising and baffling discrepancy exists between theoretical and swarm-derived experimental cross sections for vibrational excitation of H_2 at energies up to roughly 1·0 eV—a discrepancy made more puzzling by the excellent agreement for this excitation between the theoretical cross sections and data obtained in low-energy beam measurements. In an effort to shed some light on this mystery, we have tried (in Section 7) to play 'devil's advocate' to the experimental and theoretical research here reported, discussing potential weaknesses in each study. We conclude, however, that a serious conundrum remains.

2. Swarm Experiments and Their Analysis

The technique for deriving momentum-transfer and inelastic cross sections from swarm experiments* is now well established (Huxley and Crompton 1974 and

* The momentum-transfer cross section usually derived from swarm experiments is the *total* momentum-transfer cross section (i.e. the sum of the elastic and inelastic contributions). In molecular gases at low energies the cross section is dominated by the elastic momentum-transfer cross section. We use 'integral' rather than 'total' for the cross section defined by $\int \mathrm{d}\sigma/\mathrm{d}\Omega \, \mathrm{d}\Omega$, where $\mathrm{d}\sigma/\mathrm{d}\Omega$ is the differential cross section for scattering through Ω, in order to reserve 'total' for the sum of pure and ro–vibrational cross sections (see Section 6.1) or the sum of elastic and inelastic cross sections, either integral or momentum-transfer (see Section 6.3).

references therein). Essentially, it consists of measuring as many physical properties as possible of an electron swarm that is in a quasi-steady state determined by a balance between the power input from an electric field and the energy dissipation rate in collisions between the electrons and the neutral gas. A procedure summarised in Fig. 1 is then used to determine a set of cross sections that is consistent with the experimental data. In the first step, transport or rate coefficients are inferred from measurements of current, frequency, radiant flux, pressure, temperature, etc. The same coefficients are then calculated from an appropriate set of trial cross sections and the results compared with the experimentally determined coefficients for all values of E/N (the ratio of electric field strength to gas number density) for which measurements were made. After suitable adjustments are made to the initial set, a final set of cross sections is obtained for which the calculated transport coefficients match the experimental data to within experimental error over the entire range of E/N.

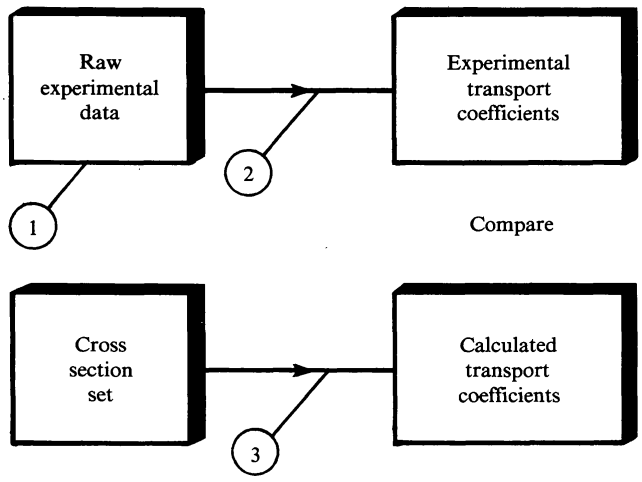

Fig. 1. Flow chart showing steps in the derivation of a set of cross sections consistent with the results of swarm experiments.

The calculation of the transport and rate coefficients first requires solving the linear Boltzmann equation to determine the electron velocity distribution function. Approximate, and sometimes adequate, descriptions of the experimental situation (when there is no ionisation or attachment, at least) can be obtained by assuming: (i) that the distribution function $F(r, c, t)$, describing the instantaneous density of electrons at position r with velocity c, is separable into a spatially-dependent density function $n(r, t)$ and a spatially-independent velocity distribution function $f(c, t)$, that is, $F(r, c, t) = n(r, t) f(c, t)$; and (ii) that $f(c, t)$ can be represented by the two leading terms of an expansion in spherical harmonics—the so-called 'two-term approximation' (Huxley and Crompton 1974). In the steady state $[f(c, t) \equiv f(c)]$ the formulae for the drift velocity v_{dr}, the transverse diffusion coefficient D_T, and the

rate coefficient k_j for the jth excitation process are then

$$v_{\mathrm{dr}} = -\frac{eE}{3N}\left(\frac{2}{m}\right)^{\frac{1}{2}} \int_0^\infty \frac{\epsilon}{\sigma_{\mathrm{m}}(\epsilon)} \frac{\mathrm{d}}{\mathrm{d}\epsilon} f_0(\epsilon)\, \mathrm{d}\epsilon, \tag{1}$$

$$D_{\mathrm{T}} = \frac{1}{3N}\left(\frac{2}{m}\right)^{\frac{1}{2}} \int_0^\infty \frac{\epsilon}{\sigma_{\mathrm{m}}(\epsilon)} f_0(\epsilon)\, \mathrm{d}\epsilon, \tag{2}$$

$$\kappa_j = \left(\frac{2}{m}\right)^{\frac{1}{2}} \int_0^\infty \epsilon \sigma_j(\epsilon) f_0(\epsilon)\, \mathrm{d}\epsilon, \tag{3}$$

where $\sigma_{\mathrm{m}}(\epsilon)$ is the total (elastic+inelastic) momentum-transfer cross section, $\sigma_j(\epsilon)$ is the integral cross section for the jth excitation process, and $f_0(\epsilon)$ is the leading (symmetric) term in the velocity distribution function with a change of variable to the energy ϵ. In this paper the parameter E/N, which determines the velocity distribution function, is expressed in terms of the townsend unit [1 townsend (Td) $= 10^{-21}$ V m^2].

The formulation described above is adequate in many circumstances, particularly when cross sections are required to be found from swarm measurements in pure gases such that they are *consistent* with the data but are not necessarily the 'true' cross sections, and these cross sections are to be used subsequently to predict the electrical characteristics of mixtures. Also, because of its simplicity, this formulation is useful for explanatory purposes. However, when cross sections of maximum accuracy are to be unfolded from swarm data, or when the accuracies of cross sections derived from other sources are to be tested, a more rigorous formulation is required. Analytical treatments are now available that properly account for non-conservative processes (i.e. attachment and ionisation—see, for example, Tagashira 1981; Ness and Robson 1986; Robson and Ness 1986 and references therein), while for conservative situations, such as the present case, there are solutions of Boltzmann's equation that account for density gradients and avoid the two-term approximation (Kumar *et al.* 1980 and references therein; Pitchford and Phelps 1982; McMahon 1983; Segur *et al.* 1983). Where necessary the new generation of transport theory has been applied to the analysis described in this paper.

The foregoing paragraphs contain a formal description of the principles underlying the extraction of cross sections from experimental swarm data. The following qualitative discussion may help to elucidate this procedure.

For a given set of experimental conditions the cross sections within an energy range spanning the maximum in the energy distribution function determine that function and hence the properties of the swarm.* Because the distribution function, and particularly the position of its maximum, can be changed by varying the electric field, the energy dependence of the cross sections can be probed by measuring the swarm parameters over a range of applied field strengths. This point is illustrated in Fig. 2, which shows the momentum-transfer cross section $\sigma_{\mathrm{m}}(\epsilon)$ for molecular hydrogen, the cross section $\sigma_{\mathrm{r}(0,2)}$ for the rotational transition $j_0 = 0$ to $j = 2$, and the cross section $\sigma_{\mathrm{v}(0,1)}$ for the vibrational transition $v_0 = 0$ to $v = 1$. On the same

* The range often includes the threshold region of the next accessible inelastic process, even though relatively few of the higher energy electrons have energies exceeding the threshold energy.

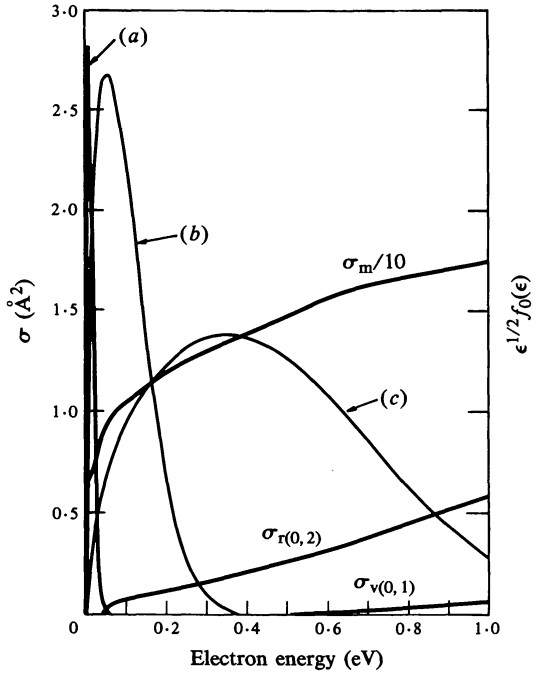

Fig. 2. Unnormalised electron energy distribution functions in para-hydrogen at 77 K for three values of E/N [(*a*) 0·01 Td; (*b*) 1·0 Td; (*c*) 7·0 Td] in relation to the cross sections for momentum transfer σ_m, rotational excitation $\sigma_{r(0,2)}$, and vibrational excitation $\sigma_{v(0,1)}$. [From Crompton (1983).]

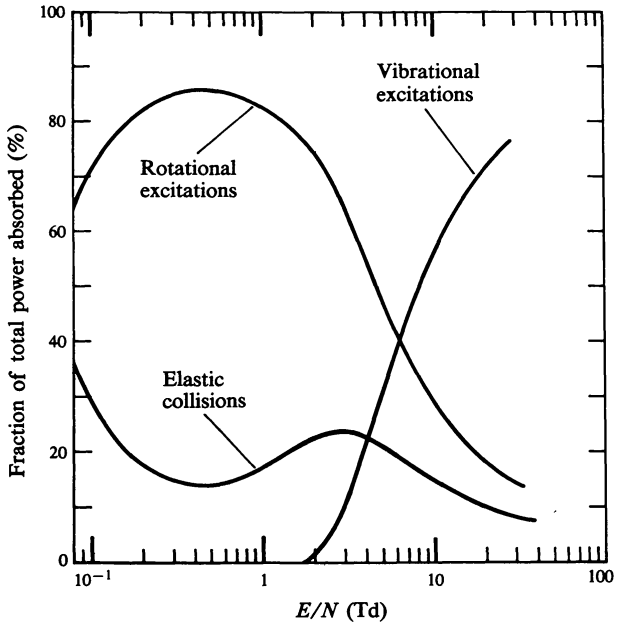

Fig. 3. Fractions of the total power absorbed in elastic collisions and in rotational and vibrational excitation in para-hydrogen at 77 K plotted as functions of E/N. [From Crompton *et al.* (1969).]

energy scale the energy distribution functions in para-hydrogen at 77 K are plotted for $E/N = 0{\cdot}01$, $1{\cdot}0$ and $7{\cdot}0$ Td. At the lowest value of E/N very few electrons have energies above the rotational threshold ($\sim$45 meV). The swarm characteristics (i.e. the energy distribution function and transport coefficients) are then largely determined by $\sigma_m(\epsilon)$, and since the position of the maximum of the distribution function depends on E/N, these characteristics are most sensitive to $\sigma_m(\epsilon)$ in a band of energies that can be varied by changing E/N. For this reason the energy dependence of $\sigma_m(\epsilon)$, but of no other cross section, can be determined over a limited energy range by analysing the experimental data for low values of E/N.

At and somewhat below the intermediate value of E/N shown in Fig. 2, very few electrons have energies above the vibrational threshold, but a large fraction of the total number in the swarm can excite molecular rotation. Because about 45 meV of energy is lost as a consequence of each rotational excitation, compared with a small fraction of a millivolt in each elastic collision, the dominant energy loss process in this range of E/N is rotational excitation. This is illustrated in Fig. 3, which shows the fractions of the input power dissipated in elastic collisions and in collisions which excite rotation and vibration. Because of the dominance of rotational excitation in the intermediate range of E/N, the energy dependence of the rotational cross section can be found by analysing experimental data in this range.

At the highest value of E/N a significant fraction of the electrons in the swarm can excite both rotation and vibration and, because of the much larger energy loss associated with vibrational excitation, the latter process rapidly dominates as E/N increases (see Fig. 3—from Crompton *et al.* 1969). It follows that the cross section for vibrational excitation can be found by analysing the experimental data at these higher values of E/N.

If energy transfer in elastic collisions were solely responsible for the influence of these collisions on the swarm characteristics, one might expect that the range of E/N over which one could extract elastic cross section data would be restricted to those values for which a negligible fraction of the electrons in the swarm has energies exceeding the rotational threshold (see Fig. 2), leading to a correspondingly narrow range of energy over which the cross section could be determined. However, the total momentum-transfer cross section appears explicitly in the formulae for the transport coefficients (equations 1 and 2). Consequently, if the inelastic cross sections are small by comparison with the elastic cross section (as for e–H_2 scattering below 1 eV where their sum is less than 4% of the elastic cross section), a small error only is made in equating the *elastic* momentum-transfer cross section to the *total* momentum-transfer cross section derived from the swarm analysis. Thus the elastic cross section can be determined over the full energy range covered by the energy distributions of the swarms even though, at the higher swarm energies, the elastic energy losses are a small fraction of the total.

In monatomic gases, for experimental conditions such that the fraction of the electrons in the swarm able to produce electronic excitation is negligible (that is, for lower values of E/N), elastic scattering is the sole energy-loss mechanism. The elastic momentum-transfer cross section can therefore be determined from measurements of a single transport coefficient (the drift velocity) and confirmed by measurements of another (the transverse diffusion coefficient); see, for example, Crompton *et al.* (1967). But the accuracy of this technique, which is based on analysis of data for a single

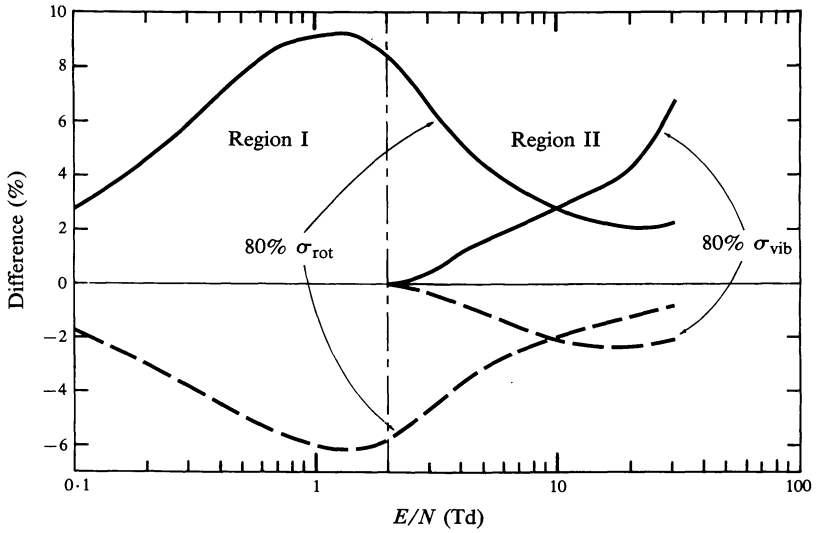

Fig. 4. Effect on the calculated electron transport coefficients in para-hydrogen of reducing by 20%, in turn, the rotational and vibrational cross sections of Fig. 2: full curves, percentage changes in D_T/μ ($\mu = v_{dr}/E$); dashed curves, percentage changes in v_{dr}. The ratio D_T/μ is measured more commonly than D_T in swarm experiments (see e.g. Huxley and Crompton 1974).

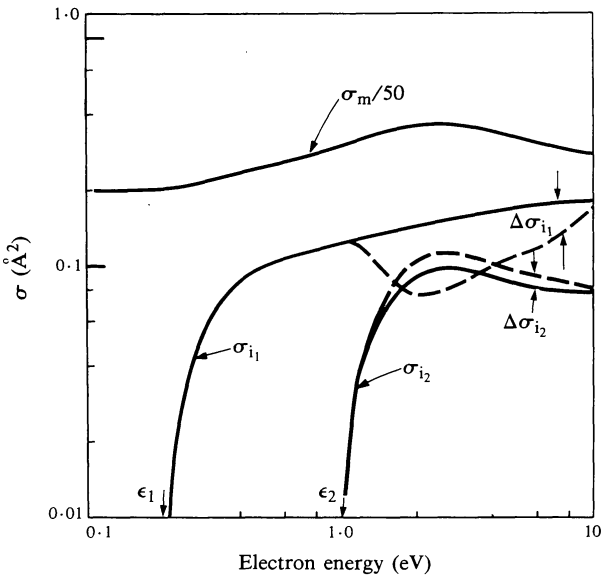

Fig. 5. Pairs of inelastic cross sections that would lead to transport coefficients that were indistinguishable experimentally. The pairs of cross sections are shown as full and dashed curves.

coefficient, is reduced when a feature of the cross section has a width that is comparable with the spread of the distribution functions used to determine it. This is the case for argon whose cross section has a Ramsauer–Townsend minimum (Milloy *et al.* 1977).

The situation is less favourable for molecular gases. As mentioned above, the effects of elastic and inelastic processes on the transport coefficients are often separable. Such a separability enables the elastic momentum-transfer cross section to be determined from drift and diffusion data with an accuracy that compares favourably with that of cross section data obtainable from other experimental techniques, although this accuracy falls short of the very high accuracy achievable for the monatomic gases in the most favourable circumstances. However, even in this situation, the *inelastic* cross sections determined from drift and diffusion data alone lose uniqueness if a significant fraction of electrons in the swarm have energies that enable them to excite more than one inelastic process. We can illustrate this point in two ways.

First, we reduce by 20%, in turn, the rotational and vibrational cross sections of Fig. 2, and calculate the change in the transport coefficients. The results are shown in Fig. 4, where the changes are expressed as percentages of the original values. Three important points are demonstrated here:

(1) Reducing the vibrational cross sections $\sigma_{v(0,1)}$ and $\sigma_{v(0,2)}$ has no discernible effect on the calculated transport coefficients in the range of E/N from 0 to 2 Td, which we shall call region I. Consequently, when adjusting the cross section set to fit measured transport data in this region, changes to the momentum-transfer and rotational-excitation cross sections alone influence the calculated transport coefficients. Therefore cross sections determined from an analysis of transport data have a high order of uniqueness and accuracy at energies at which they significantly influence the transport coefficients in region I. The energy range extends from threshold to about 0·35 eV.

(2) For E/N above 2 Td, which we shall call region II, the changing importance of rotational and vibrational excitation is apparent. The effect of rotation diminishes, and one cannot determine the rotational cross section uniquely above about 0·35 eV because of the competing influence of vibrational excitation.

(3) Although the effect of rotation becomes smaller with increasing E/N, it never becomes negligible. Therefore, unlike the rotational cross section, the vibrational cross section can never be determined uniquely in the threshold region without knowing the rotational cross section there reasonably accurately.

Second, we examine the 'cross-talk' between the two inelastic cross sections in the following example. Let us assume that there are two inelastic processes with cross sections $\sigma_{i_1}(\epsilon)$ and $\sigma_{i_2}(\epsilon)$ and associated excitation energies ϵ_1 and ϵ_2, where $\epsilon_2 > \epsilon_1$, and that both $\sigma_{i_1}(\epsilon)$ and $\sigma_{i_2}(\epsilon)$ contribute negligibly to the momentum-transfer cross section $\sigma_m(\epsilon)$* (see Fig. 5). We also assume a large molecular mass so we can neglect energy exchange in elastic collisions.

If all the molecules are in the ground state, i.e. there are no collisions of the second kind (superelastic collisions), the rate of energy transfer to the molecules through collisions of electrons with energy ϵ is given by

$$N(2/m)^{\frac{1}{2}}\epsilon^{\frac{1}{2}}\{\sigma_{i_1}(\epsilon)\epsilon_1+\sigma_{i_2}(\epsilon)\epsilon_2\}, \tag{4}$$

because we have assumed negligible energy exchange in elastic collisions.

* For the purpose of this discussion, scattering is taken to be isotropic; the total and momentum-transfer cross sections are therefore equal.

Now suppose that an arbitrary change $\Delta\sigma_{i_1}(\epsilon')$ is made to $\sigma_{i_1}(\epsilon)$ at an energy $\epsilon' > \epsilon_2$. It follows from equation (4) that a change of $\Delta\sigma_{i_2}(\epsilon')$ to $\sigma_{i_2}(\epsilon)$ such that

$$\Delta\sigma_{i_2}(\epsilon') = -(\epsilon_1/\epsilon_2)\Delta\sigma_{i_1}(\epsilon')$$

would nullify the change to $\sigma_{i_1}(\epsilon)$ because it would not alter the rate of energy transfer. This argument enables us to construct pairs of model gases which would be virtually indistinguishable in experiments where only electron transport coefficients (i.e. drift velocities and diffusion coefficients) were measured. An example is shown in Fig. 5. Both model gases have the same momentum-transfer cross section, while the inelastic cross sections (shown by the full and dashed curves) have been chosen so that at each energy $\Delta\sigma_{i_2}(\epsilon) = -(\epsilon_1/\epsilon_2)\Delta\sigma_{i_1}(\epsilon)$.

The situation just described is clearly relevant to the problem of unravelling inelastic (and elastic) cross sections from experimental transport data, where the 'cross-talk' is the basic cause of the uniqueness problem alluded to above.

This example is also useful in illustrating how the problem can be solved (in principle) when data for an appropriate rate coefficient can be measured (see e.g. Bulos and Phelps 1976; Lawton and Phelps 1978; Tachibana and Phelps 1979; Buckman and Phelps 1985).

If, for example, the rate coefficient κ_2 for the second inelastic process of our model could be measured as a function of E/N, then we could use these data to discriminate between the two inelastic processes. Although the cross section sets represented by the full and dashed curves in Fig. 5 yield the same distribution functions and hence the same transport coefficients, the calculated rate coefficients κ_2 clearly differ because κ_2 explicitly depends on $\sigma_2(\epsilon)$ (see equation 3). We shall have more to say about the problem of uniqueness in Section 3.

The conceptual simplicity of crossed-beam or absorption-type beam experiments on the one hand, and the complexity of the interpretation of swarm experiments in terms of collision processes on the other, may lead one to underestimate the problems associated with cross section determinations from the former and to be overly skeptical of claims made for the latter. In the following sections we illustrate the basic limitations of swarm experiments and how some of these limitations may be removed by appropriate synthesis of theory and experiment. But we shall not repeat the reasons why swarm experiments play an essential role despite these limitations, nor discuss the problems associated with making absolute cross section measurements in beam experiments, for several reviews have addressed these issues (Crompton 1983; Trajmar *et al.* 1983). Nevertheless, the following points are worth repeating to place the limitations of swarm techniques in proper perspective.

First, every scattering event is fully accounted for in a swarm experiment. In beam experiments, particularly crossed-beam experiments, there are inherent difficulties in measuring the distribution of electrons scattered in the forward and backward directions, or of otherwise properly accounting for these scattering events in determining integral cross sections.

Second, in most swarm experiments static gas samples at relatively high pressures are used. The electrons of the swarm therefore interact with a neutral gas whose number density can be accurately measured, a feature that is essential if absolute cross sections are to be determined. In absorption-type beam experiments the collision

chamber is part of a dynamic gas flow system in which the pressure is less than 10^{-3} Torr (≡0·133 Pa). The technical difficulty of determining the absolute number density along the collision path is of a different order from that associated with swarm experiments. In crossed-beam experiments the problem of determining the number density in the neutral beam is such that, with rare exceptions, normalisation must be used to obtain absolute cross sections (see e.g. Trajmar *et al.* 1983).

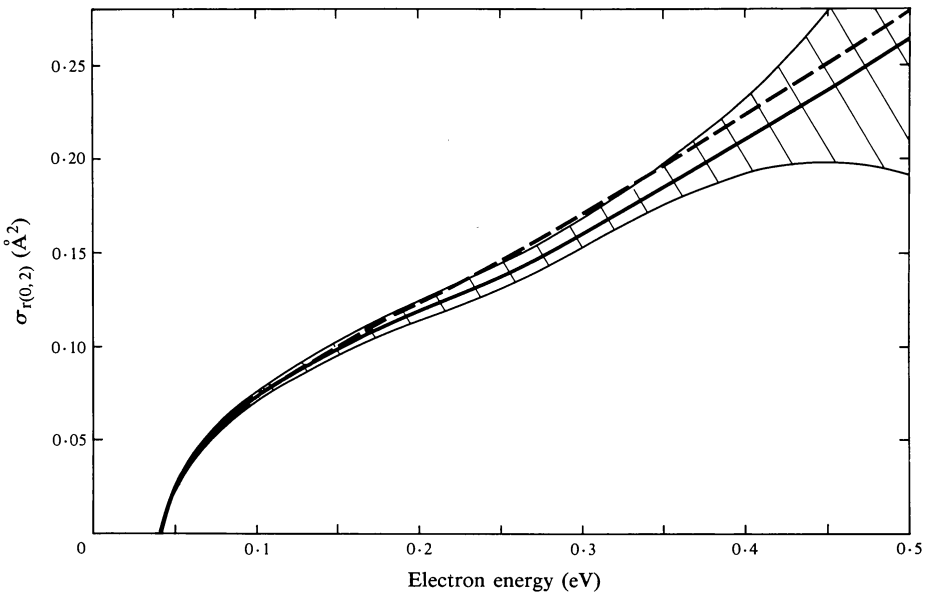

Fig. 6. Comparison of the theoretical $j_0 = 0$ to $j = 2$ rotational-excitation cross section with that derived from the swarm analysis. The estimated experimental uncertainty is shown by the cross-hatched region.

Finally, determining the details of the energy distribution of the electrons in a swarm experiment—that is, the most probable energy and the width of the distribution—is an integral part of the analysis and, as is well known, swarms of millivolt electrons are as easy to control as those of several eV. In contrast, establishing an absolute energy scale for electrons in the millivolt range remains a formidable problem for crossed-beam experiments [although time-of-flight techniques have provided a solution for absorption-type experiments (Ferch *et al.* 1980, 1985; Buckman and Lohmann 1986)], *while the distribution of electron energies within the beam is rarely accounted for, even though it may be significant.*

With the exception of the first, these problems do not amount to fundamental limitations on beam experiments, and great progress has been made in recent years toward their solution. Nevertheless, in assessing the present status of theory and experiment, one should keep in mind that swarm experiments provide the only source of experimental data for absolute near-threshold cross sections for which credible estimates of experimental error exist.

3. Swarm-derived Cross Sections for Pure Rotational Excitation and Their Extrapolation above the Vibrational Threshold

As discussed above, analysis of transport coefficients in para-hydrogen at 77 K for intermediate values of E/N enables $\sigma_{r(0,2)}$ to be determined from threshold to an energy approaching the vibrational threshold ($\sim$0·5 eV) without recourse to other experimental or theoretical data. Crompton *et al.* (1969) showed that this cross section could be determined with an estimated uncertainty of $\pm 5\%$ up to 0·3 eV, although this uncertainty rapidly increases for larger energies. No advances since then have resulted in a revision of the cross section or its error bounds, and it remains the experimental benchmark with which to compare the new theoretical results of Morrison *et al.* (1984*b*).

The comparison is made in Fig. 6, which shows the theoretical cross section (dashed curve) and a cross-hatched area within which this cross section would have to lie to be compatible with the transport data and the error bounds assigned to them. The rapidly widening error bounds as energy increases result from the rapidly growing influence of vibrational excitation in the analysis and consequent loss of uniqueness (see Section 2). Clearly the theoretical cross section is not only consistent with the experimental transport data, but the agreement between the best estimate of the cross section from the swarm analysis (full curve) and the theoretical cross section is remarkable. The sensitivity of the transport data to the rotational-excitation cross section is demonstrated by the error bounds that can be assigned to the swarm-derived cross section ($\pm 5\%$) from the claimed experimental uncertainties ($\pm 1\%$ for v_{dr} and $\pm 2\%$ for D_T/μ) over the range of E/N most sensitive to rotational excitation. This has been discussed in detail by Crompton *et al.* (1969).

In Section 6 we will compare in detail theoretical cross sections with available experimental data. Our immediate purpose is to construct a rotational-excitation cross section of sufficient accuracy that it can be used to derive the vibrational cross section (Section 4). To do so we need only note that at energies from threshold to about 0·3 eV, where the swarm analysis of transport data in para- and normal hydrogen provides unique rotational-excitation cross sections for the $j_0 = 0$ to $j = 2$ and $j_0 = 1$ to $j = 3$ transitions, the agreement between theory and experiment is satisfactory. Since the theoretical rotational cross sections are expected to be equally accurate from threshold to (at least) 8 eV (see Section 5) we can use the theoretical $\sigma_{r(0,2)}$ to extrapolate the experimental cross section beyond 0·3 eV. In practice, we found the best agreement between calculated and measured transport coefficients when we reduced the theoretical cross section by 7%, which is the difference between the theoretical and swarm-derived cross sections at 0·3 eV. The uncertainty in the *vibrational* cross section unfolded from the transport data that results from this uncertainty in the *rotational* cross section will be discussed in Section 4.1.

4. Upgrading the Transport Analysis for H_2 by a Synthesis of Theory and Experiment: Swarm-derived Vibrational Cross Section

In the original papers describing the derivation of elastic and inelastic cross sections from transport data in normal and para-hydrogen (Crompton *et al.* 1969; Crompton *et al.* 1970) three areas were identified as requiring further attention, although no significant changes to the cross sections were expected to result from any improvement in the analysis. These areas were:

(i) the extrapolation of the rotational cross sections above 0·3 eV, which was previously based on the rigid-rotator cross sections of Henry and Lane (1969);

(ii) the splitting of the total vibrational cross section into its rotationally elastic and inelastic components;

(iii) the transport theory used to analyse the data, which was previously based on the two-term approximation (see Section 2).

The new theoretical work described in the following section enables us to deal satisfactorily with (i) and (ii), while the development of transport theories that avoid the two-term approximation also enables us to eliminate this approximation as even a small source of error.

4.1 Effect on the Swarm-derived Vibrational Cross Section of Uncertainty in the Rotational Cross Section

In Section 2 we discussed the loss of uniqueness in the transport analysis when two inelastic channels are energetically accessible to higher energy electrons in the swarm and showed that one could compensate for changes in the cross section with the smaller threshold by making smaller changes in the other cross section. This greatly facilitates our analysis of para-hydrogen transport data to obtain the vibrational cross section, because the ratio of the threshold energies is greater than 10 : 1.

As we have seen, in the energy range from threshold to 0·3 eV, where the swarm-derived rotational cross section $\sigma_{r(0,2)}$ is unique, theory and experiment agree to within 7% (see Fig. 6). Since the accuracy of the theoretical results should improve as the energy increases from threshold to a few eV, $\pm 10\%$ may be taken as a reasonable estimate of the uncertainty of the cross section at higher energies. With this uncertainty, application of the scaling factor described in Section 2 shows the uncertainty in $\sigma_{v(0,1)}$ arising from $\sigma_{r(0,2)}$ to be less than 10%.

4.2 Effect of Rotational Splitting

In earlier swarm analyses the effect of rotational excitation accompanying vibrational excitation was neglected, that is, a single vibrational-excitation cross section was assumed with an associated energy loss of 0·52 eV. The resulting cross section was therefore the sum of the rotationally elastic and inelastic cross sections and was subject to a small error arising from failure to account for the larger energy loss ($\sim 10\%$) associated with simultaneous rotational excitation. The new theoretical work described in Section 5 provides cross sections for both pure vibrational and ro–vibrational excitation. The cross sections of most significance to the present determination of the cross sections for the vibrational transition $v_0 = 0$ to $v = 1$ are $\sigma_{rv(00,01)}$ and $\sigma_{rv(00,21)}$, with threshold energies of 0·516 and 0·558 eV respectively. Knowing these cross sections, we can remove a source of error in the earlier analysis by using the energy-dependent ratio of the theoretical rotationally elastic to inelastic cross sections as a known parameter in the swarm analysis. This procedure leaves a single unknown: the energy dependence of either cross section.

This refinement lowers the total vibrational cross section by about 5%. As will be shown in Section 6.3 the agreement between the swarm cross sections and theory is unsatisfactory. Nevertheless, even if the theoretical rather than the experimental cross sections ultimately require revision, it is unlikely that a change in the *ratio* of the theoretical cross sections would be large enough to significantly affect the swarm-derived cross section.

4.3 Transport Theory beyond the Two-term Approximation

Except for the work of Haddad and Crompton (1980), the analyses of transport coefficients in hydrogen and mixtures containing hydrogen have been carried out using numerical solutions of Boltzmann's equation based on the two-term approximation. General arguments (see e.g. Lin *et al.* 1979) show that this approximation is unlikely to lead to serious error, because in the energy range of interest the inelastic e–H_2 cross sections are small compared with the elastic cross section. For para-hydrogen, a comparison of the values of the transport coefficients calculated using the two-term theory with converged values obtained by the moment method of Lin *et al.* (1979) shows the error in the two-term values of v_{dr} to be negligible, and errors in D_T/μ to increase from zero to 1·4% as E/N increases from zero to 30 Td. Anisotropic scattering was assumed in these calculations; with isotropic scattering the maximum error was slightly less (1·2%).

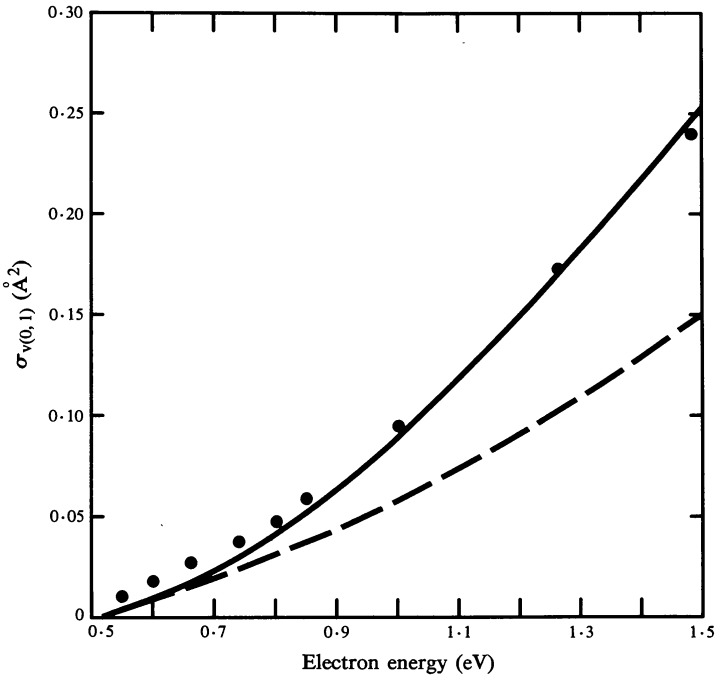

Fig. 7. Cross sections for (total) vibrational excitation from $v_0 = 0$ to $v = 1$ (i.e. ro–vibrational cross sections summed over final rotational states): theoretical (full curve); swarm-derived (dashed curve); beam data of Ehrhardt *et al.* (1968) (circles).

Although these differences are small they are significant, at least for the transport coefficient D_T/μ. We have therefore based the analysis in this paper on the higher order theory.*

* Note that the error due to the use of the two-term code becomes significant (>1%) only for E/N greater than about 10 Td. The original determination of the rotational cross section was therefore not affected by its use.

4.4 Vibrational Cross Section

The new swarm-derived vibrational-excitation cross section that results from an analysis incorporating the refinements described in the previous paragraphs is shown in Fig. 7. We reserve further discussion of it until Section 6.3, noting two points only here. First, the sum of the rotationally elastic and inelastic cross sections differs only slightly from the cross section derived earlier from the same experimental data (Crompton *et al.* 1970), half the reduction of 10% being due to the inclusion of rotational inelasticity. This was expected, because the refinements to the analysis have resulted in minor changes only to the transport coefficients calculated using a given set of cross sections. Second, the fact that the swarm-derived cross section is *lower* than the theoretical cross section rules out the possibility that the difference can be explained by failure to include the influence of an additional (unknown) inelastic process in the analysis of the swarm data. The inclusion of such a process (if it existed) would require the vibrational cross section to be further reduced in order to obtain agreement between calculated and measured transport coefficients (see Fig. 5).

5. Theoretical Calculations

5.1 Overview of Theoretical Concerns

The complexity of the electron–molecule system forces the theorist to compromise when calculating cross sections, especially at near-threshold energies. Approximations must be invoked both in constructing the interaction potential and in solving the nonrelativistic Schrödinger equation for the scattering function (for an introduction see Morrison 1983). One must balance a desire for rigour and exactitude against pragmatic concerns such as the availability of computer (and human) resources.

A primary objective of the theoretical component of this project was calculation of cross sections of an accuracy sufficient to justify their subsequent use in transport analysis (see Section 2). Consistent with this goal, we have sought high accuracy in all numerical aspects of the computation. Once the e–H_2 interaction potential was chosen and the collision theory formulated, the scattering equations were solved numerically to better than 1% for integrated and 3% for differential cross sections (for details see Morrison *et al.* 1984*a*, 1984*b*).

Because we sought to provide theoretical cross sections that might resolve discrepancies among existing experimental data, we designed a theoretical formulation that is wholly unconnected to any experimental cross sections. For example, we rejected model potentials, such as the widely-used cutoff asymptotic polarisation potential (see Lane 1980), that include a parameter requiring adjustment to experimental cross section data. We have been unable to wholly avoid model potentials; but we have designed these potentials to provide as accurate a treatment of inelastic scattering as possible (see Section 5.3).

A detailed report of our theoretical calculation will more properly appear elsewhere. But in order to gain a perspective on the comparison of theoretical and experimental cross sections in Section 6, it is necessary to briefly consider the theoretical treatment.

5.2 Collision Theory

We focus exclusively on *electronically-elastic* collisions. Hence the (energetically inaccessible) excited electronic states of the target—those above the ground $X^1\Sigma_g^+$

state of H_2—are not explicitly included in our scattering theory.* The fundamental equation of the theory can be obtained by projecting the three-electron time-independent Schrödinger equation for the system onto the (Born–Oppenheimer) electronic wavefunction for the ground state of H_2. The wavefunction that solves the resulting scattering equation depends on the spatial variables of the internuclear axis $\boldsymbol{R}$ and of the projectile $\boldsymbol{r}$, where these coordinates are defined in a space-fixed (laboratory) reference frame. For an electron of energy $k_0^2/2$ incident on a molecule in initial state $\nu_0 = (v_0 j_0 m_{j_0})$, with v_0 and j_0, m_{j_0} the vibrational and rotational quantum numbers of the initial state, the scattering equation is

$$\{\hat{T}_e(\boldsymbol{r})+\hat{\mathscr{H}}^{(n)}(\boldsymbol{R})+V_{st}(\boldsymbol{r})-E\}\,\Psi_{E\nu_0}(\boldsymbol{r},\boldsymbol{R})=0, \tag{5}$$

where $\hat{T}_e$ is the kinetic energy operator for the projectile, and $\hat{\mathscr{H}}^{(n)}$ is the nuclear Hamiltonian that results from the Born–Oppenheimer separation of the full target wavefunction. That is, $\hat{\mathscr{H}}^{(n)}$ is the sum of the nuclear kinetic energy operator (for rotational and vibrational motion) and the Born–Oppenheimer electronic energy:

$$\hat{\mathscr{H}}^{(n)}(\boldsymbol{R}) = \hat{T}^{(n)}(\boldsymbol{R})+\mathscr{E}^{(e)}_{X^1\Sigma_g^+}(\boldsymbol{R}). \tag{6}$$

The total energy E in equation (5) is

$$E = \tfrac{1}{2}k_0^2+\epsilon_{v_0 j_0}. \tag{7}$$

The potential energy in equation (5), $V_{st}(\boldsymbol{r})$, is just the average over the ground electronic state of the sum of two-particle bound–free electrostatic interactions between the projectile and the constituent particles of the target. Sensibly, this potential is called the static potential:

$$V_{st}(\boldsymbol{r}) = \left\langle X^1\Sigma_g^+ \left| -\frac{1}{|\boldsymbol{r}-\frac{1}{2}\boldsymbol{R}|}-\frac{1}{|\boldsymbol{r}+\frac{1}{2}\boldsymbol{R}|}+\sum_{i=1}^{2}\frac{e^2}{|\boldsymbol{r}-\boldsymbol{r}_i|}\right| X^1\Sigma_g^+\right\rangle. \tag{8}$$

But equation (5) is not adequate to describe the scattering of low-energy electrons, for it neglects the indistinguishability of the projectile and target electrons (exchange effects) and induced distortions of the target by the projectile (polarisation effects). When exchange is treated exactly (by antisymmetrising the full three-electron system wavefunction before projecting out the ground electronic state of the target) an additional, non-local potential energy operator $\hat{V}_{ex}$ appears in equation (5). In many applications, however, the non-local nature of this operator renders solution of the resulting scattering equations impractical, and it is replaced by a local model exchange potential (see Section 5.3*b*).

Polarisation effects are equally unwieldly. In quantum collision theory, these effects arise from virtual electronic excitations (Castillejo *et al.* 1960), so they cannot

* Except where otherwise stated, atomic units ($\hbar = m_e = c = a_0 = 1$) are used here and in Section 7.

rigorously be included in the present formulation, in which closed electronic states are not included. Instead, we incorporate target polarisation via a parameter-free model potential $V_{\rm pol}$ (see Section 5.3*c*). Thus, to allow for exchange and polarisation in low-energy electron–molecule collisions we replace $V_{\rm st}(r)$ in equation (5) by the full static–exchange–polarisation (SEP) interaction potential

$$V_{\rm sep} = V_{\rm st} + \hat{V}_{\rm ex} + V_{\rm pol}\,. \tag{9}$$

From the asymptotic behaviour of the function $\Psi_{Ev_0}(r, R)$—or more precisely of the radial scattering functions obtained from this function by a succession of eigenfunction expansions (see Sections 5.2*a* and 5.2*b*)—we obtain the scattering matrix from which we calculate various cross sections. It is in the determination of the scattering matrix that approximations enter the collision theory itself.

The optimum representation for calculation of the scattering matrix is one that explicitly acknowledges that neither the rotational angular momentum of the target j nor the orbital angular momentum of the projectile l is conserved in the scattering process. It is therefore preferable to formulate electron–molecule scattering theory in the coupled angular momentum representation (Arthurs and Dalgarno 1960), in which these angular momenta are coupled (via the Clebsch–Gordan series) to give the total angular momentum $J = j + l$. In this representation, radial scattering functions and S matrices are labelled by the quantum number J, which corresponds to the operator J^2. (This observable and the projection J_z of J on the space-fixed z axis are constants of the collision.) In the coupled angular momentum representation, the scattering matrix is $S^J_{vjl,v_0j_0l_0}$.

Differential and integrated cross sections are conveniently expressed in terms of a related matrix, the T-matrix:

$$T^J_{vjl,v_0j_0l_0} \equiv \delta_{v,v_0} - S^J_{vjl,v_0j_0l_0}\,, \tag{10}$$

where $v = (v_j\, m_j)$. For example, the integrated cross section for excitation from initial state $v_0 j_0$ to final state vj is

$$\sigma(v_0 j_0 \to vj) = \frac{\pi}{k_0^2(2j_0+1)} \sum_J (2J+1) \sum_{l,l_0} |\, T^J_{vjl,v_0j_0l_0}|^2\,. \tag{11}$$

The elastic momentum-transfer cross section (for $v_0 = 0$, $j_0 = 0$),

$$\sigma_{\rm m} = \int \frac{{\rm d}\sigma}{{\rm d}\Omega}\,\Bigg|_{v_0j_0 \to v_0j_0} (1 - \cos\theta)\,{\rm d}\Omega\,, \tag{12a}$$

which is of primary concern in the analysis of swarm experiments, is expressed in terms of elements of the T matrix as

$$\sigma_{\rm m} = \frac{\pi}{k_0^2} \sum_{J=0}^{\infty} \{(2J+1)|\, T^J_{00J,00J}|^2 - (J+1)(T^{J*}_{00J,00J}\, T^{J+1}_{00J+1,00J+1} + T^J_{00J,00J}\, T^{J+1*}_{00J+1,00J+1})\}\,. \tag{12b}$$

The first task of the theorist studying inelastic scattering is to solve the Schrödinger equation (5) for the S matrix.* In practice, serious problems beset this chore. These problems arise from the dynamical interaction between the quantum motion of the nuclei and that of the electron that is responsible for ro–vibrational excitations (Lane 1980, Morrison 1983 and references therein). Mathematically, this interaction is manifested in the non-separability of the wavefunction $\Psi_{E\nu_0}(\boldsymbol{r}, \boldsymbol{R})$. That is, the dependence of this function on the nuclear variables $\boldsymbol{R}$ cannot rigorously be separated from its dependence on the projectile variables $\boldsymbol{r}$. Consequently, equation (5) cannot be transformed into separate equations for the nuclear motion and for the scattering function.

5.2a Inelastic Collisions

To treat this coupling correctly we would expand $\Psi_{E\nu_0}(\boldsymbol{r},\boldsymbol{R})$ in two complete sets of eigenfunctions, thereby reducing the partial differential equation (5) to a set of coupled single-variable ordinary differential (or, if exchange is included exactly, integro-differential) equations. The necessary eigenfunction expansions are

[1] expansion in the set of eigenfunctions $\{\chi_\nu(\boldsymbol{R})\}$ of the nuclear Hamiltonian $\hat{\mathscr{H}}^{(n)}$, which are complete in the rotational and vibrational variables of the nuclei;

[2] expansion in the set of spherical harmonics $Y_l^{m_l}(\hat{\boldsymbol{r}})$—eigenfunctions of l^2 and l_z—which are complete in the angular variables of the electron.

For a diatomic molecule, the nuclear target functions are simple products of rotational functions [spherical harmonics $Y_j^{m_j}(\hat{\boldsymbol{R}})$] and vibrational functions [solutions $\phi_v(R)$ of the nuclear Schrödinger equation of the target].

These expansions assume a slightly different form if, as is usually the case, we work in the coupled angular momentum representation. In this formulation, we use the Clebsch–Gordan series to combine the rotational functions $Y_j^{m_j}(\hat{\boldsymbol{R}})$ of the target with the spherical harmonics $Y_l^{m_l}(\hat{\boldsymbol{r}})$ to form coupled angular functions $\mathscr{Y}_{jl}^{JM}(\hat{\boldsymbol{r}}, \hat{\boldsymbol{R}})$. The resulting expansion basis of *lab-frame close-coupling* (LFCC) theory simply consists of products of these coupled angular functions and vibrational functions $\phi_v(R)$. From the coefficients in this expansion—which are obtained by solving coupled equations in the single variable r—we obtain the scattering matrix.

The important point for the present study is that in this formulation the dynamical interaction of the motion of the nuclei and of the projectile is included exactly via the coupled scattering equations. So if we solve a sufficient number of these equations to converge the cross sections, these results should reflect fully this interaction.

This procedure is straightforward but, in general, intractable. The plethora of nuclear target states that are coupled by $\hat{\mathscr{H}}^{(n)}$ and the large number of partial waves that are coupled by the non-spherical interaction potential $V_{sep}(r)$ give rise to large sets of coupled equations that must be solved simultaneously. To date, fully converged ro–vibrational cross sections have been obtained for only one system: e–H_2.

We use the LFCC formulation to calculate cross sections for which a precise treatment of the nuclear dynamics seems to be vital: ro–vibrational cross sections.

* In practice, we solve for the K matrix. The advantage of the K matrix is that it is defined by real boundary conditions, rather than the complex form that defines the S matrix. It is a trivial matter to determine the T matrix from the K matrix and thence cross sections such as those in equations (12).

But to simplify the resulting computational chores, we avoid *integro*-differential equations by approximating the non-local exchange operator $\hat{V}_{ex}$ in equation (9) by a local model-exchange potential that is optimised for the excitations of interest (see Section 5.3*b*).

5.2*b* *Elastic Collisions*

At scattering energies below about 10 eV, the integrated (and differential) total and momentum-transfer cross sections are dominated by the elastic contribution. Fortunately, the computation of elastic cross sections that take account of target vibration can be simplified—with no loss of accuracy—by using the adiabatic-nuclei (AN) approximation (Chase 1956; Hara 1969; Faisal and Temkin 1972; Shugard and Hazi 1975).

A great deal has been written recently about the AN method, including a tutorial-style introduction (Morrison 1983), so little need be said here. The underlying idea of the method is analogous to the Born–Oppenheimer separation in studies of bound states of molecules. Although the dependence of $\Psi_{E\nu_0}(\boldsymbol{r}, \boldsymbol{R})$ on nuclear variables $\boldsymbol{R}$ cannot *rigorously* be separated from its dependence on the scattering variables $\boldsymbol{r}$, in the AN method we introduce such a separation as an approximation. Specifically, we approximate this function by the product of a nuclear wavefunction for the initial target state (ν_0) and an *adiabatic* scattering function. The latter represents the continuum state of the projectile in an (imaginary) environment in which the nuclear geometry of the target is fixed for the duration of the collision. The adiabatic scattering function depends on the nuclear coordinates only *parametrically*. This simplification allows the projectile to respond *adiabatically* to changes in the nuclear geometry, so one can calculate approximate elastic and ro–vibrational eross sections.

In practice, AN calculations are not performed in the space-fixed (laboratory) reference frame of Section 5.2*a*, but rather in a body-fixed frame, in which the polar coordinate axis is fixed along the internuclear axis $\hat{\boldsymbol{R}}$. Once nuclear and projectile variables have been separated, the nuclear coordinates and quantum numbers disappear from the AN scattering equations. These body-frame fixed-nuclei equations can therefore be reduced to coupled radial equations by expanding the adiabatic scattering function in spherical harmonics, which are complete in the angular coordinates of the projectile (defined with respect to the internuclear axis).

The asymptotic dependence of the solutions of these equations yields a scattering matrix that, when transformed back into the coupled angular momentum (laboratory) representation, becomes an approximation to $S^J_{vjl,v_0j_0l_0}$, from which approximate cross sections can be calculated.

5.3 *Interaction Potential*

The electron–molecule interaction potential (9) contains three components—static, exchange, and polarisation—each of which depends on r, θ and R. The R dependence of this potential increases markedly the computer time needed to study vibrational excitation, for each of these components must be evaluated at a large number of internuclear geometries. This complication makes model potentials for the exchange and polarisation terms irresistible.

5.3a Static Contribution

The dominant short-range interaction in electron–molecule scattering is the static potential $V_{st}(r)$. This term arises from the Coulomb interactions of the projectile and the target (see equation 8). Our procedure for evaluating this static potential from the Hartree–Fock electronic wavefunction of the target is straightforward and efficient (Morrison 1980). First one evaluates the one-particle density function $\rho(r, \theta)$ from the variationally-optimised molecular orbitals (the $1\sigma_g$ orbital for H_2) and then expands this function in Legendre polynomials. From the resulting radial expansion coefficients, the static potential can easily be calculated (Schmid *et al.* 1980).

In the present implementation, we solved the Hartree–Fock equations for H_2 at 11 internuclear separations ranging from $R = 0{\cdot}5a_0$ to $2{\cdot}6a_0$ using a [5s2p/3s2p] contracted basis of nucleus-centred gaussian-type orbitals (Morrison *et al.* 1984*b*). One measure of the accuracy of our static potential is the average of the theoretical quadrupole moment function $q(R)$ over the ground vibrational state, $\langle \Phi_0 | q(R) | \Phi_0 \rangle$. Using vibrational wavefunctions calculated by solving the nuclear Schrödinger equation with our near-Hartree–Fock electronic energy $\mathscr{E}^{(e)}_{X^1\Sigma_g^+}(R)$, we obtain for this quantity the value $-0{\cdot}4704ea_0^2$, which compares quite favourably with the experimental value $-0{\cdot}474\pm0{\cdot}034ea_0^2$ (MacAdam and Ramsey 1972).

5.3b Exchange Contribution

As noted in Section 5.2, exchange effects, if treated exactly, give rise to integral terms in the coupled radial scattering equations of either the LFCC or body-frame fixed-nuclei formulations. In recent years several numerical techniques for solving the fixed-nuclei integro-differential equations have been implemented (Collins *et al.* 1980; Collins and Schneider 1981). The solution of these equations is computationally tractable because the number of coupled channels in this formulation—and hence the number of simultaneous integro-differential equations that one must solve—is reduced considerably, the nuclear states having been removed from the scene by the AN approximation. We take advantage of this fact in our calculation of elastic cross sections, for which the AN approximation is quite accurate, by treating exchange exactly for this scattering process.

But because we use the LFCC formulation for inelastic scattering (see Section 5.2), we must accommodate coupling of numerous rotational and vibrational states and of several partial waves. To somewhat simplify this calculation, we incorporate exchange for inelastic scattering via a model exchange potential, thereby eliminating the need to contend with integro-differential equations.

The particular model potential we have used has been exhaustively studied and shown to be viable for a wide range of electron–molecule systems (see Collins and Morrison 1982 and references therein). The form of this potential, which was originally used for e–H_2 scattering by Hara (1967), can be obtained from the exact non-local exchange kernel by implementing two approximations (Morrison and Collins 1978): a free-electron-gas (FEG) treatment of the target electrons, and the Born approximation for the scattering function. The resulting form of this FEG potential is

$$V_{ex}(r; R) = -\frac{2}{\pi} k_F(r; R)\left(\tfrac{1}{2} + \frac{1-\eta^2}{4\eta} \ln\left|\frac{1+\eta}{1-\eta}\right|\right). \qquad (13a)$$

In this equation, the Fermi wavenumber is defined as

$$k_F(r; R) \equiv \{3\pi^2 \rho(r; R)\}^{\frac{1}{3}}. \tag{13b}$$

The parameter η is defined in terms of the local wavenumber

$$k(r; R) \equiv \{2(E_b + I) + k_F^2(r; R)\}^{\frac{1}{2}} \tag{13c}$$

as

$$\eta \equiv k/k_F. \tag{13d}$$

Notice that E_b in equation (13c) is the body energy—the energy at which the body-frame fixed-nuclei equations are solved—so the FEG exchange potential (13a) is energy-dependent. In Hara's original formulation, I was chosen to be the ionisation potential of the target.

Studies of Hara's form of the FEG exchange potential revealed that, as one might expect from the approximations on which it is based, this model was less accurate for a two-electron target than for a many-electron target, such as CO_2. But its accuracy for systems with few target electrons can be markedly improved by replacing I in equation (13c) by a function of R that is chosen so that model-exchange results at a single scattering energy reproduce those calculated in exact-exchange calculations (Morrison and Collins 1978). This gambit gives rise to the tuned free-electron-gas exchange (TFEGE) potential used in the present study. This name is perhaps a misnomer: like all parts of our interaction potential, the exchange component is not adjusted to experimental data. Rather the 'tuning' is to another theoretical calculation. We now describe how $I(R)$ is chosen.

In the body-frame fixed-nuclei formulation, two quantities are conserved in the scattering event: the projection Λ of the projectile's orbital angular momentum l along the internuclear axis, and the parity η of the scattering function with respect to inversion through the midpoint of that axis.* Hence the coupled body-frame fixed-nuclei scattering equations separate into sets according to the values of these quantum numbers. Thus, we solve scattering equations in the Σ_g symmetry ($\Lambda = 0$ and η = even), the Σ_u symmetry ($\Lambda = 0$ and η = odd), and so forth. Each such set of equations gives rise to a scattering matrix for that symmetry and hence to a 'partial cross section' $\sigma_{\Lambda,\eta}$. The integrated cross section in this theory, summed over all final rotational states, is evaluated from these partial cross sections as

$$\sigma_{tot} = \sum_{\Lambda,\eta} \sigma_{\Lambda,\eta} = \sigma_{\Sigma_g} + \sigma_{\Sigma_u} + \ldots. \tag{14}$$

However, the relevant quantity for our tuning procedure is not the partial cross section but the eigenphase sum.

Eigenphase sums play a role in electron–molecule scattering theory analogous to that of phase shifts in potential scattering theory. Because partial waves are coupled by the non-spherical electron–molecule interaction potential, phase shifts *per se* cannot be defined. Instead, the K matrix in a particular electron–molecule symmetry (i.e.

* Note that only in the fixed-nuclei formulation is the projection Λ a collision constant. If the rotational Hamiltonian is included in the body-frame scattering equations, coupling with respect to Λ appears (Chang and Fano 1972).

for a particular Λ and η) is diagonalised and then the arctangent of the resulting eigenvalues calculated. The sum of these 'eigenphases' is denoted $\delta_{\text{sum}}^{\Lambda,\eta}$. We tune the eigenphase sum rather than the partial cross section because the former is particularly sensitive to the interaction.

Here is how it's done. The function $I(R)$ is determined at each R *in a single electron–molecule symmetry at a single scattering energy*. Thus, the body-frame fixed-nuclei scattering equations *in the static-exchange approximation*—i.e. with polarisation neglected for the moment—are solved at a given R and at the 'tuning energy' E_b with exchange treated exactly. These equations are then solved using the model-exchange potential (13a), and $I(R)$ is determined so that the eigenphase sums in the symmetry of choice from the two calculations agree to three decimal places.

To apply this strategy to inelastic e–H_2 scattering, we exploit the fact that when ro–vibrational e–H_2 cross sections are broken down into their constituent symmetry contributions, the Σ_u symmetry emerges as dominant at energies from threshold to about 5 eV (Morrison *et al.* 1984*b*). Therefore we tune the Σ_u eigenphase sum. We choose as the tuning energy $E_b = 0{\cdot}54$ eV, a value just above the threshold for the $v_0 = 0 \rightarrow v = 1$ excitation. The resulting $I(R)$ is optimum for ro–vibrational excitation at energies from threshold to several eV (Morrison and Saha 1986).

Two features of the TFEGE potential should be emphasised. First, once tuning has been carried out (in a single symmetry at a single energy), the resulting function $I(R)$ is used for all electron–molecule symmetries at all scattering energies. That is, the tuning procedure is not energy- or symmetry-dependent. Second, this procedure does not entail any adjustment to match experimental cross section data; i.e. our use of the TFEGE cannot bias the theoretical results in favour of one or another experimental data set.

5.3c Polarisation Component

The final term in the interaction potential is the polarisation potential. As noted in Section 5.2, once we have jettisoned closed electronic states from our scattering theory, we cannot include polarisation exactly. [Notwithstanding recent progress in this area (Schneider and Collins 1983; Gibson *et al.* 1984) an exact treatment of polarisation for ro–vibrational excitation remains beyond the power of present-day computers.] Hence, once again, we resort to a model potential.

In designing a parameter-free model polarisation potential, several aspects of polarisation must be taken into consideration. The polarisation potential has a deceptively simple asymptotic form: in the limit that the projectile is very far from the target, we have

$$V_{\text{pol}}(r; R) = -\frac{\alpha_0(R)}{2r^4} - \frac{\alpha_2(R)}{2r^4} P_2(\cos\theta) \qquad (r \rightarrow \infty), \tag{15}$$

where $\alpha_0(R)$ and $\alpha_2(R)$ are the spherical and non-spherical polarisabilities of the target.

At non-asymptotic values of r, however, the nature of the polarisation distortion is not so simple. Provided the projectile is outside the target charge cloud, this distortion can be treated as an adiabatic response to the electric field of a fixed projectile. The resulting adiabatic polarisation effects have been shown to produce substantial deviations from equation (15) for some electron–molecule systems (Morrison and Hay 1979).

The situation becomes even more complicated once the projectile penetrates the target charge cloud. In this region of space, non-adiabatic (velocity-dependent) effects may play a role, as do quantum-mechanical phenomena that lie outside a single-particle theory such as the one implemented here—e.g. bound–free correlation effects. These complicated short-range effects are the principal difficulty in treating polarisation in charged-particle scattering.

We have implemented (Gibson and Morrison 1984) a model polarisation potential that treats adiabatic polarisation effects exactly, since it is based on a variational calculation of the decrease in the total energy of the system due to the induced polarisation distortion (Lane and Henry 1968). This model incorporates non-adiabatic effects approximately using a non-penetrating approximation that was first introduced by Temkin (1957) in a study of electron–atom scattering. In this approximation, the adiabatic polarisation potential near the target is weakened by the *ad hoc* expedient of 'switching off' the bound–free Coulomb interactions whenever the radial coordinate of the projectile is less than a radial coordinate of either target electron.

Investigation of the resulting polarisation potential, which we have dubbed the BTAD ('better-than-adiabatic dipole') potential, has shown it to be quite accurate for e–H_2 and e–N_2 scattering in the rigid-rotator approximation (Morrison *et al.* 1984*a*). It is important to note that the BTAD potential does not contain any adjustable parameters. Like the other components of our interaction potential, it is not biased in favour of a particular experiment.

Table 1. Theoretical and experimental H_2 polarisabilities (in a_0^3)

	Hartree–Fock[A]	CI[B]	Experimental
α_0	5·376	5·472	5·4265[C]
α_2	1·410	1·394	1·3567[D]

[A] Present study. [B] Kolos and Wolniewicz (1967).
[C] Newell and Baird (1965). [D] MacAdam and Ramsey (1972).

Detailed discussions of the BTAD polarisation potential, both for rigid-rotator calculations at the equilibrium geometry and for vibrational excitation, have appeared elsewhere (Gibson and Morrison 1984; Morrison *et al.* 1984*b*). A measure of the accuracy of this potential is given by the average of the polarisability functions $\alpha_0(R)$ and $\alpha_2(R)$ over the ground vibrational state target function. In Table 1 our values for these parameters are compared with those calculated by Kolos and Wolniewicz (1967), who used a very accurate configuration-interaction (CI) electronic wavefunction for H_2, and with experiment.

6. Comparison of Theoretical and Experimental Cross Sections

6.1 Integral Inelastic Cross Sections

In Section 4 we compared theoretical and swarm-derived cross sections for the pure rotational excitation $j_0 = 0 \rightarrow j = 2$ (Fig. 6) and for the total vibrational excitation $v_0 = 0 \rightarrow v = 1$ (Fig. 7). The theoretical results for these excitations and for pure rotational-excitation in ortho-hydrogen, $j_0 = 1 \rightarrow j = 3$, are given in Table 2, which includes energies above those shown in the figures.

Table 2. Theoretical integral cross sections versus energy for pure rotational and total vibrational excitation of H_2

ϵ (eV)	$\sigma_{r(0,2)}$ (Å^2)	$\sigma_{r(1,3)}$ (Å^2)	$\sigma_{v(0,1)}$ (Å^2)	ϵ (eV)	$\sigma_{r(0,2)}$ (Å^2)	$\sigma_{r(1,3)}$ (Å^2)	$\sigma_{v(0,1)}$ (Å^2)
0·047	0·018	—	—	0·900	0·555	0·320	0·063
0·050	0·025	—	—	1·000	0·634	0·366	0·089
0·060	0·041	—	—	1·100	0·714	0·414	0·118
0·070	0·052	—	—	1·200	0·796	0·463	0·150
0·075	0·056	0·007	—	1·400	0·958	0·560	0·218
0·080	0·060	0·013	—	1·500	1·036	0·607	0·254
0·090	0·067	0·021	—	1·600	1·112	0·652	0·289
0·100	0·073	0·026	—	1·800	1·250	0·736	0·354
0·150	0·100	0·046	—	2·000	1·370	0·809	0·407
0·160	0·105	0·050	—	2·500	1·585	0·940	0·476
0·180	0·114	0·056	—	3·000	1·704	1·014	0·483
0·200	0·124	0·062	—	3·500	1·755	1·046	0·464
0·300	0·171	0·092	—	4·000	1·758	1·050	0·432
0·400	0·222	0·122	—	4·500	1·732	1·035	0·394
0·500	0·279	0·156	—	5·000	1·689	1·010	0·356
0·520	0·291	0·174	0·001	6·000	1·579	0·945	0·288
0·540	0·305	0·172	0·003	7·000	1·461	0·876	0·234
0·560	0·315	0·177	0·004	8·000	1·349	0·809	0·193
0·620	0·354	0·200	0·011	9·000	1·247	0·748	0·161
0·700	0·408	0·232	0·023	10·000	1·156	0·693	0·136
0·800	0·480	0·275	0·041				

In Fig. 8, the cross sections $\sigma_{r(1,3)}$ are compared with swarm-derived results and with the beam data of Linder and Schmidt (1971). These authors determined cross sections from ratios of scattering intensities for elastic and inelastic scattering measured in a crossed-beam apparatus at incident energies $\epsilon_0 \geqslant 1{\cdot}5$ eV. Their apparatus encompassed an angular range from 20° to 120°, and so to determine the results in Fig. 8 the differential cross sections were extrapolated to $\theta = 0$ and 180° and the resulting function of θ numerically integrated. Linder and Schmidt normalised the sum of their integral cross sections to the measured data of Golden *et al.* (1966).* The energy resolution of the apparatus used by Linder and Schmidt was 30–40 meV, and the quoted uncertainty in their cross sections ranges from 30% at 0·3 eV to 10% at 4·0 eV.

At low energies (Fig. 8*a*) the theoretical $\sigma_{r(1,3)}$ values agree with the swarm-derived cross sections for which the estimated uncertainty is ±5% for $\epsilon < 0{\cdot}3$ eV. As the energy increases, the theoretical results gradually merge with the beam data (Fig. 8*b*)—a trend we saw in the total vibrational cross sections $\sigma_{v(0,1)}$ of Fig. 7.

6.2 Differential Cross Sections

Comparisons of theoretical and beam data are best made via *differential* cross sections, which do not require extrapolation. Moreover, differential cross sections are more sensitive than integral cross sections to assumptions and models used

* Bedersen and Kieffer (1971) analysed the experiment of Golden *et al.* (1966) and suggested an error limit of ±10% for their cross sections.

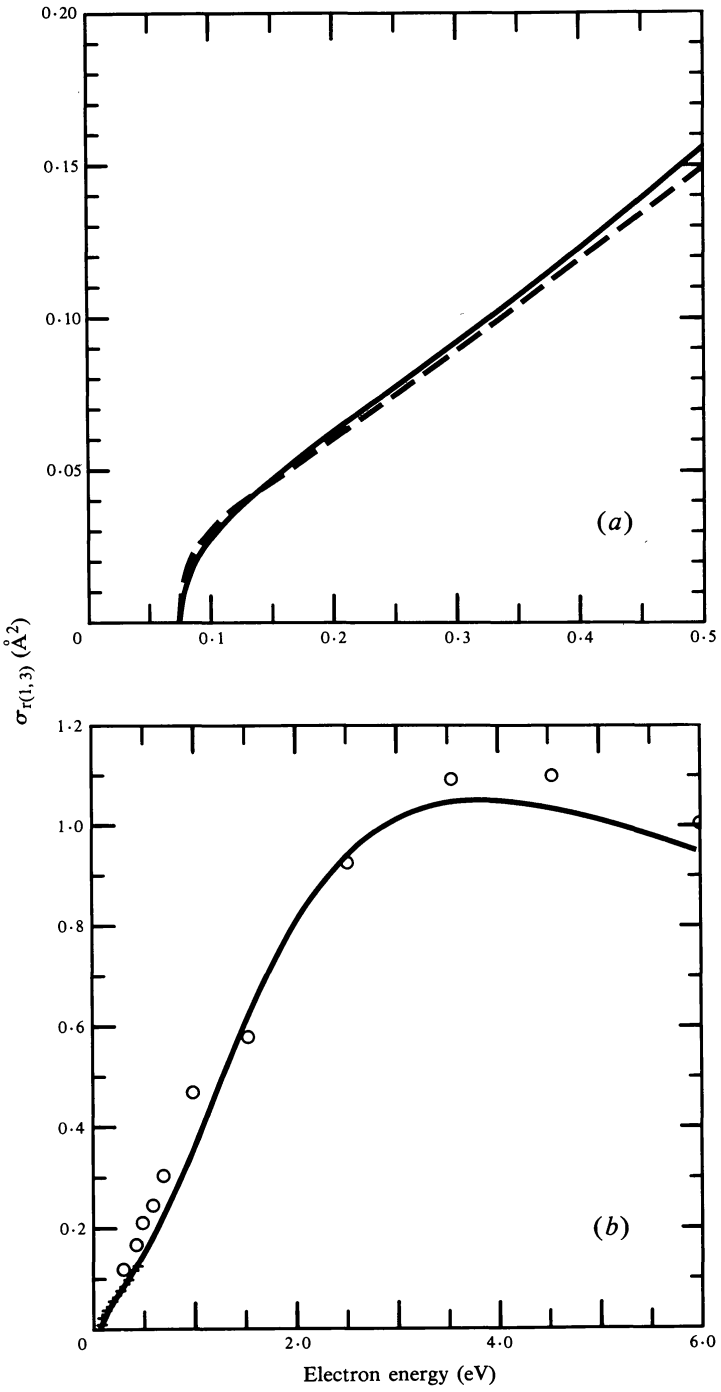

Fig. 8. Theoretical (solid curve) and experimental cross sections for the pure rotational excitation $j_0 = 1 \rightarrow j = 3$. Experimental data in (*a*) are from the swarm analysis of transport data (dashed curve) and in (*b*) from beam experiments of Linder and Schmidt (1971) (circles) and swarm analysis (crosses).

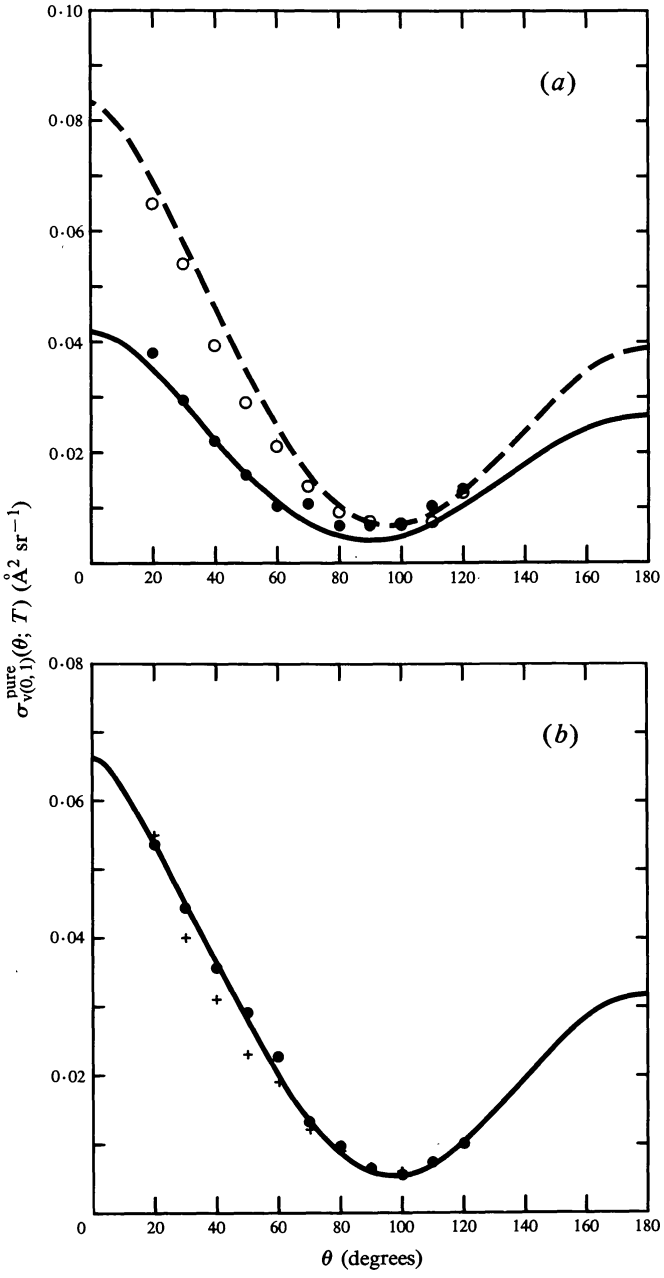

Fig. 9. Theoretical cross sections for pure vibrational excitation from $v_0 = 0$ to $v = 1$ ($\Delta j = 0$) at (*a*) 1·5 eV (solid curve and solid circles) and 2·5 eV (dashed curve and open circles), and at (*b*) 4·5 eV. The symbols in (*a*) and the solid circles in (*b*) are experimental data of Linder and Schmidt (1971). The crosses in (*b*) are data of Wong and Schulz (1974).

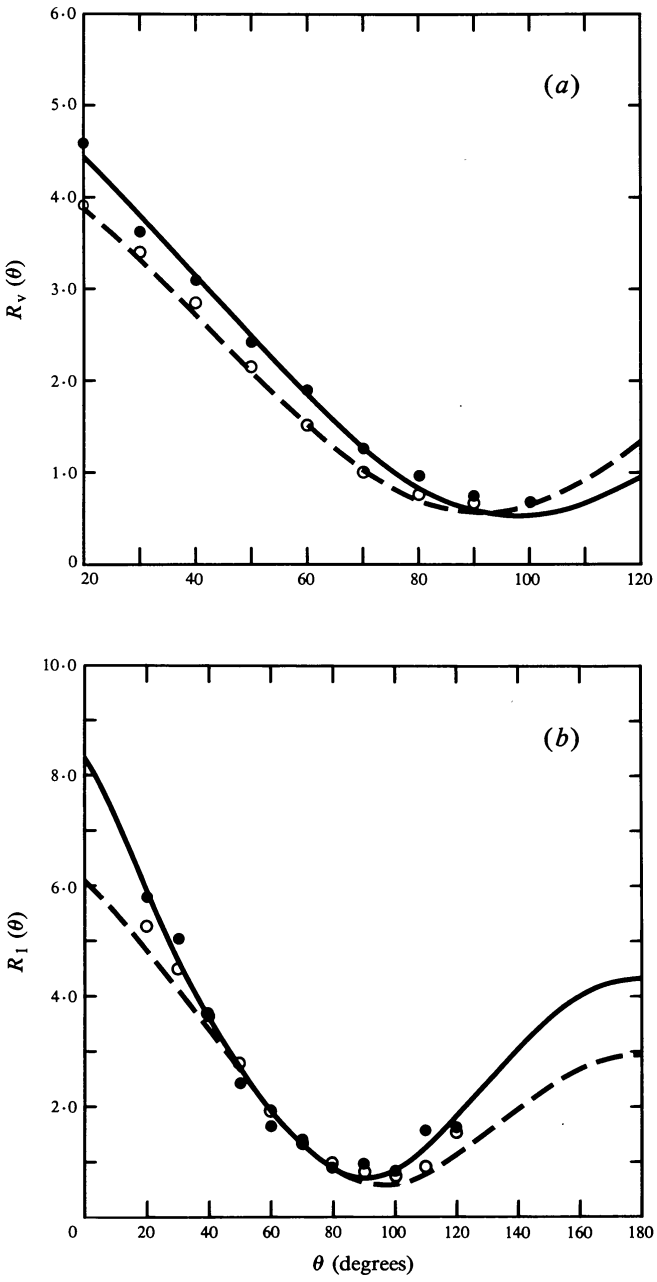

Fig. 10. Ratios of the pure vibrational cross section for $v_0 = 0 \rightarrow v$ (equation 12) to the ro–vibrational cross sections $\sigma_{rv(10,3v)}(\theta)$: (*a*) Comparison of theoretical ratios (curves) to data of Wong and Schulz (1974) (symbols) for $v = 1$ (solid curves and solid circles) and $v = 2$ (dashed curve and open circles) at 4·5 eV at $T = 298$ K; (*b*) comparison with data of Linder and Schmidt (1971) (symbols) for $v = 1$ at 1·5 eV (solid curve and solid circles) and 2·5 eV (dashed curve and open circles) at $T = 340$ K.

in theoretical calculations. In addition to the aforementioned results of Linder and Schmidt (1971), differential cross sections for elastic and inelastic scattering of electrons from H_2 have been measured by Wong and Schulz (1974) and, most recently, by W. K. Sohn *et al.* (personal communication 1986). In this section, we shall put the theory to the test of comparison with these authors' results.

We have described the experiment of Linder and Schmidt in Section 6.1. Wong and Schulz (1974) determined angular distributions for $v = 1$, 2 and 3 at an incident energy of 4·5 eV by measuring energy-loss spectra at angles from 20° to 100° in a crossed-beam apparatus with an energy resolution of 18–22 meV. Differential cross sections were determined by carrying out corresponding measurements for e–He scattering and normalising the results to the theoretical cross sections of LaBahn and Callaway (1970).

Of the available beam data, the closest counterparts to the total vibrational-excitation cross sections of Fig. 7, for which the disagreements between swarm-derived and theoretical results are greatest, are pure vibrational cross sections $\sigma^{\text{pure}}_{v(0,v)}$. These quantities are defined in terms of individual ro–vibrational cross sections $\sigma_{rv(j_0 0, j_0 v)}(\theta)$ (which for $v \neq v_0$ are strongly dependent on the initial rotational state j_0) as the average at temperature T over the distribution $N_{j_0}(T)$ of molecules in these rotational states, i.e.

$$\sigma^{\text{pure}}_{v(0,v)}(\theta; T) \equiv \sum_{j_0} N_{j_0}(T)\sigma_{rv(j_0 0, j_0 v)}(\theta). \tag{16}$$

In Fig. 9 we compare theoretical and measured pure vibrational cross sections for $v = 1$. In view of the discrepancy seen in Fig. 7, we consider the agreement of these differential cross sections at 1·5 eV to be noteworthy.

Table 3. Theoretical ratios $R_v(\theta)$ given by (17) for various angles and energies (in eV)

The pure vibrational-excitation cross sections at 4·5 eV were calculated using (16) with T = 298 K; at all other energies, T = 340 K was used

Angle (deg.)	$\epsilon = 1{\cdot}5$	$\epsilon = 2{\cdot}5$	$\epsilon = 3{\cdot}5$	$\epsilon = 4{\cdot}5$ ($v = 1$)	$\epsilon = 4{\cdot}5$ ($v = 2$)
0	8·329	6·048	5·417	5·175	4·829
10	7·137	5·492	5·099	4·959	4·401
20	5·703	4·803	4·553	4·425	3·883
30	4·586	4·103	3·936	3·823	3·331
40	3·598	3·381	3·276	3·173	2·733
50	2·696	2·646	2·589	2·508	2·111
60	1·909	1·949	1·924	1·860	1·524
70	1·296	1·345	1·334	1·288	1·033
80	0·909	0·893	0·881	0·851	0·700
90	0·785	0·641	0·611	0·596	0·571
100	0·929	0·611	0·547	0·546	0·657
110	1·301	0·785	0·679	0·686	0·933
120	1·834	1·116	0·962	0·973	1·345
130	2·444	1·536	1·334	1·344	1·821
140	3·046	1·974	1·730	1·738	2·230
150	3·575	2·373	2·093	2·097	2·717
160	3·983	2·686	2·380	2·381	3·042
170	4·239	2·883	2·563	2·562	3·243
180	4·329	2·954	2·260	2·620	3·316

Comparisons such as these are, however, subject to uncertainty. As noted above, the analyses carried out by Linder and Schmidt and by Wong and Schulz necessarily entailed calibration and normalisation of measured intensities. But one can compare their results with those of theory in a way that is free of these uncertainties by working with the ratio $R_v(\theta)$ of the differential cross section for pure vibrational excitation (at temperature T), equation (16), to that for ro–vibrational excitation, $\sigma_{rv(10,3v)}(\theta)$, i.e.

$$R_v(\theta) \equiv \sigma^{pure}_{v(0,v)}(\theta; T)/\sigma_{rv(10,3v)}(\theta). \quad (17)$$

Wong and Schulz (1974) published these ratios for several final vibrational states at 4·5 eV; they estimated their data for $R_v(\theta)$ to be accurate to within ±5%. In Fig. 10*a* we compare their results for $v = 1$ and 2 with ratios calculated using theoretical cross sections in equation (17) for $T = 298$ K (the temperature of their experiments). In Fig. 10*b* we show $R_1(\theta)$ at $T = 340$ K for 1·5 and 2·5 eV, and their experimental counterparts as calculated from the differential cross sections of Linder and Schmidt (1971). These theoretical ratios are given in Table 3.

Very recently, W. K. Sohn *et al.* (personal communication 1986) measured elastic and inelastic differential cross sections for a variety of electron–molecule systems using a crossed-beam electron spectrometer (Kochem *et al.* 1985) that renders accessible scattering angles from 10° to 140°. In this apparatus, the energy scale was calibrated to the e–N_2 shape resonance (Rohr 1977); in the e–H_2 measurements of Sohn *et al.* (1986) the primary beam energy was known to within 25 meV.

For the e–H_2 system, these authors have provided differential cross sections for elastic scattering and for the pure rotational excitation $j_0 = 1 \rightarrow j = 3$. Their results for the latter process at 0·2 and 0·6 eV are compared with the theoretical cross sections in Fig. 11.*

Turning to elastic scattering, we show in Fig. 12 the measured differential cross sections of Sohn *et al.* (1986) at two energies together with theoretical results calculated using the AN method with exact exchange, as described in Section 5.2*b*. This scattering process dominates the total and momentum-transfer cross sections, to which we now turn.

6.3 Total and Momentum-transfer Cross Sections

Since 1980, four groups have measured absolute total cross sections σ_{tot} for e–H_2 scatttering: Ferch *et al.* (1980), Dalba *et al.* (1980), Hoffman *et al.* (1982), and Jones (1985). (Here we take the 'total' cross section to be the sum of the elastic and all inelastic contributions.) All four experiments were transmission measurements; those of Ferch *et al.* (1980) and of Jones (1985) used time-of-flight discrimination. Individual quoted error estimates for the measured cross sections are given in the respective papers; suffice to say here that all are less than ±5%, except for the cross sections of Dalba *et al.* (1980) at the lowest energy (0·3 eV), where the quoted error is 7%. Data from these experiments are compared in Fig. 13 with theoretical total cross sections; the latter include contributions from vibrational excitation for $v = 1$ and 2 and, of course, from all contributing rotational excitations (see Table 4).

* We performed theoretical calculations over a narrow range of energies near 0·6 eV. The best agreement between theory and experiment was obtained for an incident energy of 0·62 eV. In view of the uncertainty in the primary energy in the experiments of Sohn *et al.*, the comparison in Fig. 11 is considered valid.

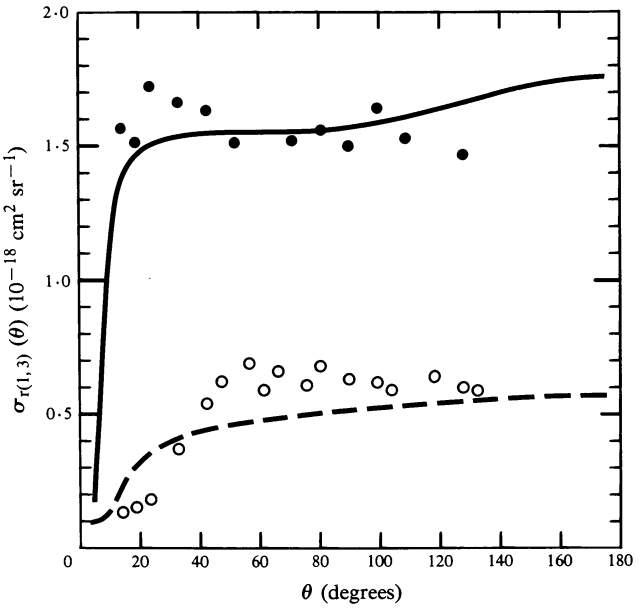

Fig. 11. Differential cross section for the pure rotational excitation $j_0 = 1 \rightarrow j = 3$ at 0·2 eV (dashed curve and open circles) and at 0·6 eV (solid curve and closed circles). The symbols are experimental data of Sohn *et al.* (1986). (The solid curve was calculated for an incident energy $\epsilon_0 = 0{\cdot}62$ eV.)

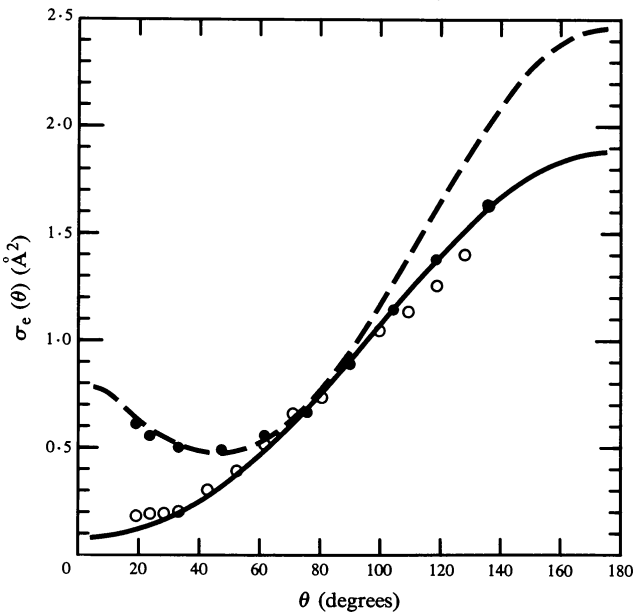

Fig. 12. Elastic differential cross sections from theoretical calculations (curves) and the experiments of Sohn *et al.* (1986) (symbols). The solid curve and open circles correspond to $\epsilon_0 = 1{\cdot}5$ eV and the dashed curve and solid circles to $\epsilon_0 = 0{\cdot}2$ eV.

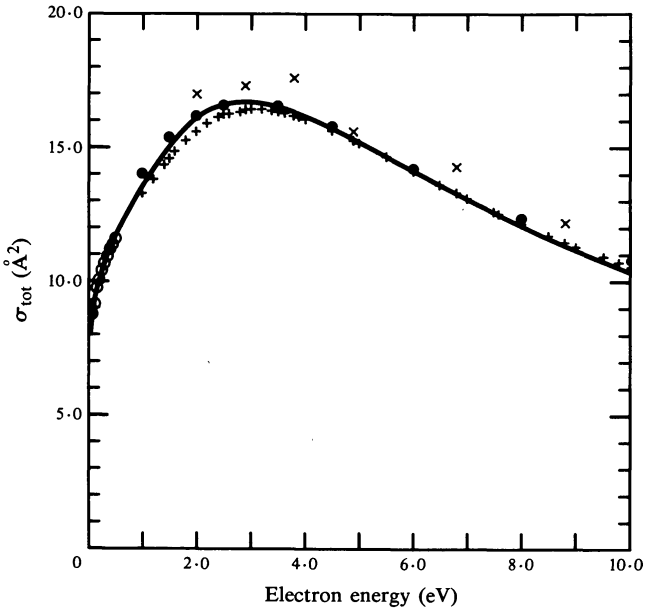

Fig. 13. Total e–H_2 cross sections (sum of elastic, rotational, and vibrational contributions) from theoretical calculations (solid curve) and the experiments of Ferch *et al.* (1980) (open circles) Dalba *et al.* (1980) (solid circles), Hoffmann *et al.* (1982) (crosses), and Jones (1985) (plusses).

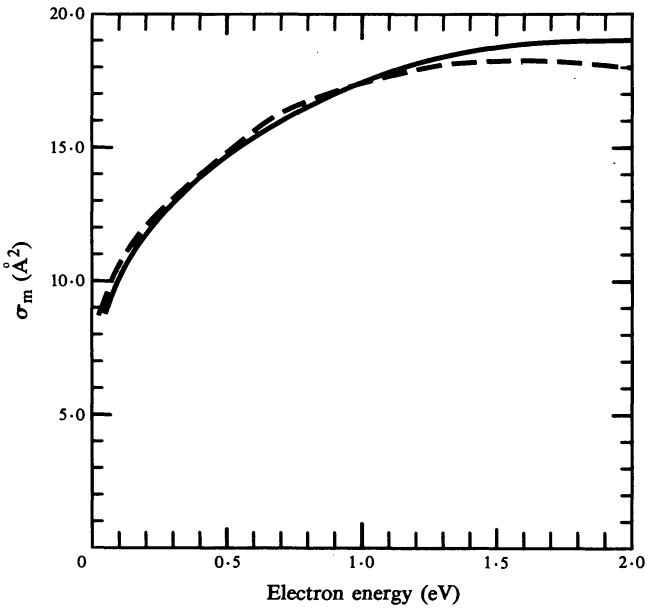

Fig. 14. Momentum-transfer cross sections for e–H_2 scattering from theory (solid curve) and swarm analysis (dashed curve).

Table 4. Theoretical total and momentum-transfer cross sections for e–H_2 scattering; rotational contributions and vibrational contributions from $v = 0$, 1, 2 and 3 are included

ϵ (eV)	σ_{tot} (Å^2)	σ_m (Å^2)	ϵ (eV)	σ_{tot} (Å^2)	σ_m (Å^2)
0·047	8·026	8·786	1·200	14·134	18·098
0·050	8·095	8·885	1·400	14·712	18·560
0·060	8·301	9·181	1·500	14·986	18·730
0·070	8·480	9·446	1·600	15·242	18·856
0·080	8·642	9·688	1·800	15·693	18·987
0·090	8·789	9·913	2·000	16·059	18·969
0·100	8·925	10·122	2·500	16·596	18·422
0·150	9·486	11·016	3·000	16·706	17·442
0·200	9·924	11·743	3·500	16·529	16·284
0·300	10·603	12·912	4·000	16·171	15·091
0·400	11·139	13·853	4·500	15·705	13·937
0·500	11·596	14·646	5·000	15·182	12·858
0·600	12·013	15·342	6·000	14·080	10·963
0·700	12·402	15·957	7·000	13·004	9·406
0·800	12·771	16·500	8·000	12·005	8·134
0·900	13·126	16·979	9·000	11·097	7·092
1·000	13·468	17·399	10·000	10·280	6·233
1·100	13·785	17·752			

In the context of the present paper, it is important to ascertain the implications, if any, of the agreement in Fig. 13 for inelastic cross sections. Doing so is rendered difficult by the dominance of the elastic contribution so, at low energies, the comparison in Fig. 13 merely indicates the accuracy of our representation for elastic e–H_2 scattering. But at higher energies, from a few eV to 10 eV, roughly 5% of this cross section is contributed by inelastic processes, so Fig. 13 does provide some insight into the accuracy of the theoretical inelastic cross sections at energies above about 1·0 eV.

Finally, we return to swarm-derived results in Fig. 14, comparing theoretical total momentum-transfer cross sections (Table 4) with those determined from transport data (see Section 2). As in the case of the total cross sections, elastic scattering dominates σ_m in this energy range.

7. Error Analysis

The comparison of vibrational-excitation cross sections in Section 6 strongly indicates the presence of error either in the theoretical calculations or the unfolding of ro–vibrational cross sections from swarm data. In this section we look closely and critically at both the theory and the analysis of the experimental data to see whether we can suggest the source of such error.

7.1 Theory

Possible sources of error in the theoretical study stem from the approximations that underlie our theoretical formulation for inelastic scattering:

[a] use of the TFEG potential to approximate exchange effects for inelastic cross sections;

[b] use of the BTAD polarisation potential to incorporate polarisation and correlation effects.

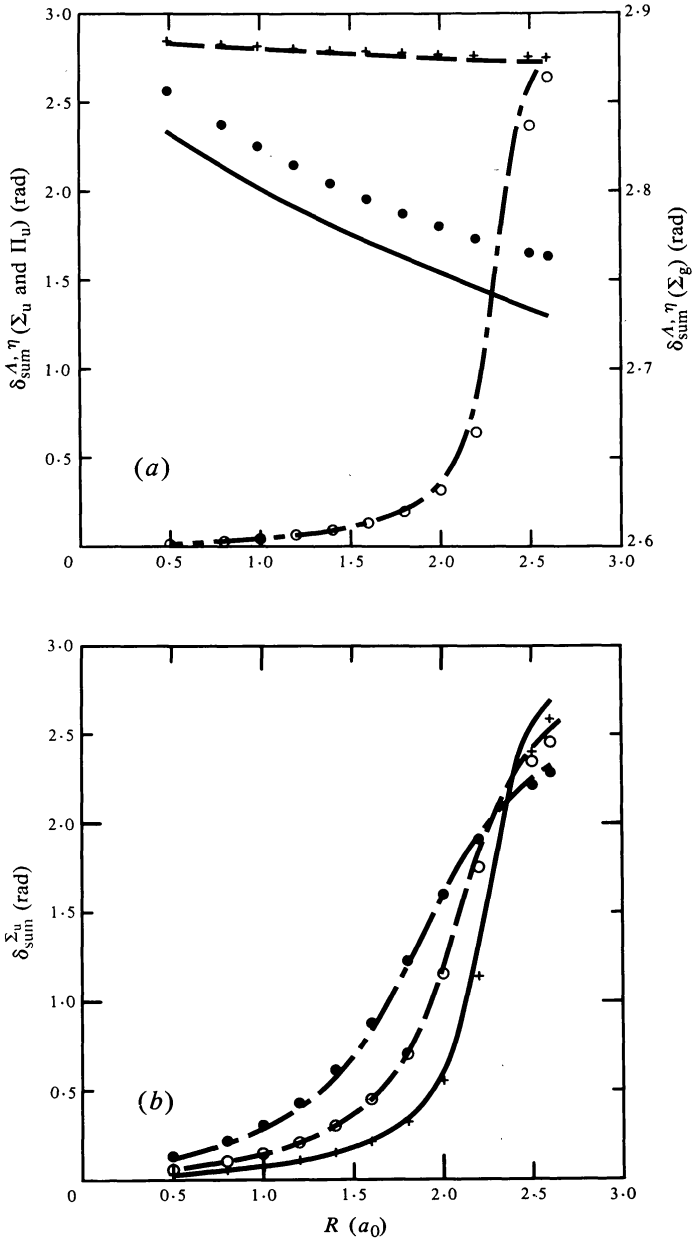

Fig. 15. Assessment of the model-exchange potential used in the theoretical calculations. Comparison of body-frame fixed-nuclei eigenphase sums versus internuclear separation R as calculated using the TFEGE model potential (Section 5.3*b*) (curves) and using an exact treatment of exchange (Collins *et al.* 1980) (symbols): (*a*) results at the 'tuning energy', 0·54 eV, which is just above the threshold for the $v_0 = 0 \rightarrow 1$ excitation, for three symmetries—Σ_g (solid curve and solid circles), Σ_u (dot–dash curve and open circles), and Π_u (dashed curve and crosses); (*b*) eigenphase sums in the Σ_u symmetry for three energies—0·08 eV (solid curve and crosses), 1·5 eV (dashed curve and open circles), and 3·0 eV (dot–dash curve and solid circles).

7.1a Exchange

Several studies have explored the accuracy of FEGE potentials for electron–molecule scattering. Morrison and Collins (1978) studied several systems at the *static-exchange* level, solving the body-frame fixed-nuclei scattering equations with exact and then with model exchange, and found that the TFEGE potential accurately mimics exchange effects in e–H_2 scattering at energies from a few tenths to several eV. Subsequently, Gibson and Morrison (1981) showed that including polarisation in the interaction potential does not vitiate this conclusion. Finally, Morrison and Collins (1981) investigated the effects of enforcing orthogonality of the scattering function to bound molecular orbitals of the same symmetry, a condition that holds rigorously in the exact static-exchange theory of scattering from a closed-shell target, and found that orthogonalisation did not change cross sections calculated with a *tuned* FEGE potential. But these studies were performed in the rigid-rotator approximation and hence shed little light on the usefulness of these potentials for vibrational excitation.

As discussed in Section 5.3*b*, we use an R-dependent FEGE potential, determined by tuning Σ_u body-frame fixed-nuclei eigenphase sums at 0·54 eV, in our LFCC calculations of ro–vibrational cross sections. The only way to quantify the accuracy of this procedure would be to repeat these LFCC calculations using an exact treatment of exchange, but could we have done so, we would not have used the model potential in the first place. Nevertheless, some insight into the validity of our model potential can be gained by seeing if it accurately 'tracks' exchange effects as the molecule vibrates.

In Fig. 15*a* we show the eigenphase sums $\delta_{\text{sum}}^{\Lambda,\eta}$ versus internuclear separation R *at the tuning energy*, 0·54 eV, in the Σ_g, Σ_u and Π_u symmetries, comparing results calculated with the TFEGE model potential to those determined when exchange is treated exactly.* *In interpreting this and subsequent figures in this section it is vital to keep in mind that the extent of the vibrational target functions for $v = 0$, 1 and 2 is (roughly) from 1·0a_0 to 2·0a_0; it is the R variation in this range that is most important to the vibrational excitations of concern in this work. It is also important to note that at energies below a few eV, vibrational-excitation cross sections are determined almost entirely by scattering in the Σ_u symmetry; only at scattering energies above roughly 5 eV do other symmetries play an important role:* Π_u *and, to a lesser extent,* Σ_g. Fig. 15*a* reveals that the TFEGE potential accurately mimics exchange effects in the Σ_u and Π_u symmetries. But the TFEGE Σ_g eigenphase sums are considerably in error. This inadequacy in our model-exchange potential is a consequence of tuning in the Σ_u rather than the Σ_g symmetry. Hence, one cannot obtain accurate *elastic* cross sections with this exchange potential. Inelastic cross sections at energies below a few eV, however, are quite insensitive to errors in the Σ_g symmetry.

In Fig. 15*b* we show $\delta_{\text{sum}}^{\Sigma_u}$ at several energies: 0·08 eV, which is near threshold for the (0, 1) → (0, 3) pure rotational excitation; 1·5 eV, where the most serious disagreement between theoretical and experimental vibrational-excitation cross sections occurs; and 3·0 eV, which is near the $^2\Sigma_u$ resonance peak in the e–H_2 cross section (Schulz 1973).

* Polarisation effects are included, via the BTAD potential discussed in Section 5.3*c*, in these results, but tuning was performed in the *static-exchange* approximation. This explains the slight differences in these comparisons for large R.

7.1b Polarisation

Calculations of electron–molecule cross sections in which polarisation effects are included at a level approaching rigor are few and far between. Only in the last few years have theorists attempted nearly exact treatments of polarisation in electron–molecule scattering (e.g. Burke *et al.* 1983; Schneider and Collins 1983; Gibson *et al.* 1984). [All of these studies are based on the rigid-rotator approximation, and in only one are non-equilibrium geometries considered (Berman *et al.* 1985).] The reason for this state of affairs is the enormous computational difficulties posed by the infinity of closed electronic target states that give rise to polarisation effects. As a consequence, it is far more difficult to assess the accuracy of our BTAD polarisation potential than our model-exchange potential, and less substantial conclusions can be drawn from comparisons that can be made with other theoretical results.

In Fig. 16 we compare our results at equilibrium with those of two other studies. Schneider and Collins (1983) used an effective optical potential to incorporate polarisation and bound–free correlation effects in rigid-rotator calculations of e–H_2 cross sections. They incorporated this potential into the body-frame fixed-nuclei scattering equations using a separable approximation and solved the resulting equations using their linear-algebraic algorithm. The principal uncertainty in this study is one that bedevils formulations based on expansions in a square-integrable basis: are the cross sections converged in basis functions—i.e. does the basis set span the relevant region of configuration space? Schneider and Collins probed this question for the Σ_g symmetry and found their optical-potential cross sections to be especially sensitive to basis set at energies below 1·0 eV, i.e. near the thresholds for ro–vibrational excitations of interest here. (A related question concerning the optical-potential approach is how to incorporate bound–free and bound–bound correlation effects in a balanced way.) These questions notwithstanding, the study of Schneider and Collins is the most accurate treatment of polarisation effects to date, and in Fig. 16 we compare their partial cross sections σ_{Σ_g} and σ_{Σ_u} at the equilibrium separation of H_2 ($1{\cdot}402\,a_0$) with those calculated using our BTAD potential. (In these calculations exchange effects were treated exactly.)

A quite different approach to polarisation was adopted by Gibson *et al.* (1984) in their implementation of the Schwinger multichannel method to e–H_2 scattering in the fixed-nuclei approximation. The Schwinger multichannel method is based on an extension of the Schwinger variational principle familiar in potential scattering theory (for a review see Lucchese *et al.* 1986). As implemented by Gibson *et al.* (1984) for e–H_2 scattering in the fixed-nuclei approximation, this method is derived from a variational functional for the scattering amplitude. This functional allows for polarisation effects using trial functions constructed from a square-integrable basis in which both open and closed electronic channels are included. Since this method entails expansion of the scattering function in L^2 basis functions, it is subject to the uncertainties discussed above. Partial cross sections calculated by Gibson *et al.* (1984) are also shown in Fig. 16.*

* Since their paper was published, these authors have discovered that neglect of π pseudo-orbitals in their expansion basis led to an incomplete representation of polarisation effects in this calculation (T. L. Gibson, personal communication). This effect may be responsible for the differences between their results and those of Schneider and Collins (1983).

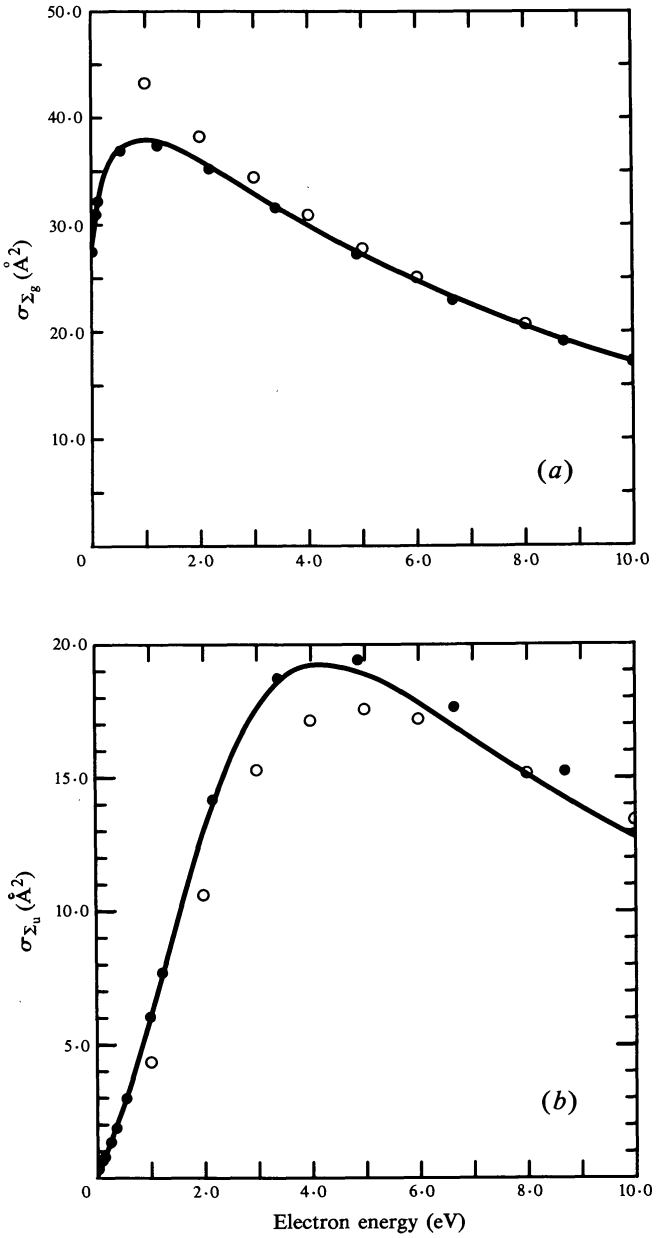

Fig. 16. Assessment of the BTAD polarisation potential in the fixed-nuclei approximation: theoretical partial cross sections for e–H_2 scattering at a fixed internuclear separation $R = R_e = 1{\cdot}402\,a_0$ in the (*a*) Σ_g and (*b*) Σ_u symmetries. Solid curves are results of the present study (see Section 5). The solid circles are cross sections from the optical-potential calculations of Schneider and Collins (1983), and the open circles are from calculations of Gibson *et al.* (1984) using the Schwinger multichannel method.

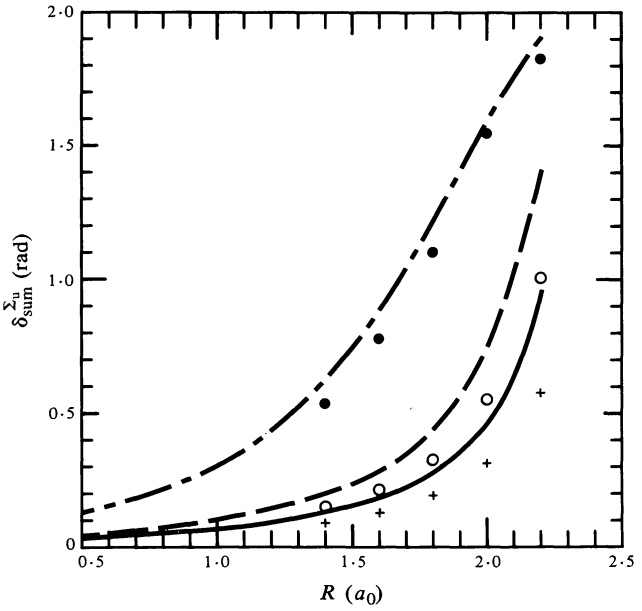

Fig. 17. Assessment of the BTAD polarisation potential for varying internuclear geometry: eigenphase sums in the Σ_u symmetry as functions of the internuclear separation R. The curves are results of the present study (see Section 5.3*c*). The symbols are data from Berman *et al.* (1985), which is based on the projection operator method and a many-body optical potential. (The latter eigenphase sums are available only for $R > R_e$.) Three energies are shown: 0·07 eV (solid curve and crosses), 1·0 eV (dashed curve and open circles), and 3·0 eV (dot–dash curve and solid circles).

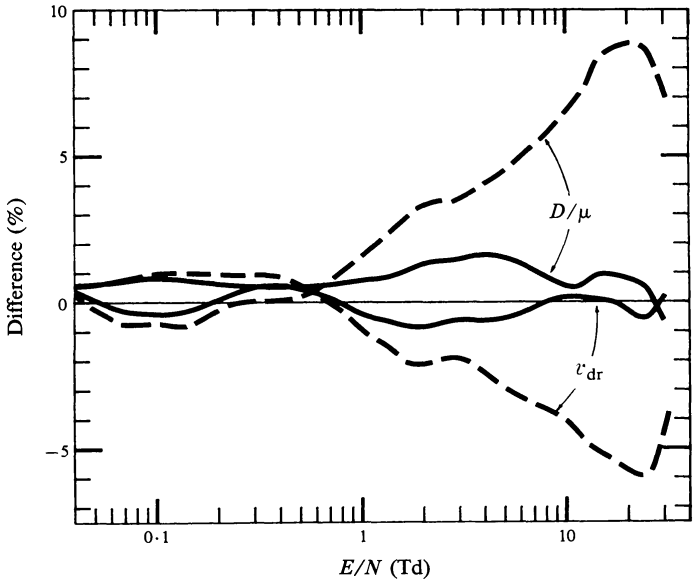

Fig. 18. Differences between the measured values of v_{dr} and D_T/μ in H_2 and those calculated using the theoretical cross sections (dashed curves). The corresponding differences when the swarm-derived cross sections are used (full curves) are shown for comparison.

Yet a third approach to polarisation was implemented by Berman *et al.* (1985) in a study of e–H_2 collisions that considered non-equilibrium geometries. These authors calculated eigenphase sums in the Σ_u symmetry (only) at several internuclear separations $R \geqslant R_{eq} = 1{\cdot}402 a_0$, using a projection operator formalism originally introduced by Feshbach (1958). Because Berman *et al.* used a many-body optical potential to transform the many-particle electron scattering problem into an equivalent one-body scattering problem, they could incorporate polarisation and correlation effects exactly up to second order in such a way that bound–bound and bound–free correlations were balanced; these features remove some of the uncertainties of the calculations discussed previously. In Fig. 17 we compare our BTAD Σ_u eigenphase sums, calculated using an exact treatment of exchange, with those of Berman *et al.* (1985). The differences between the two sets of results are difficult to interpret, because the two studies used different representations of the target and different treatments of exchange as well as different treatments of polarisation. For example, even at the static-exchange level, the results of Berman *et al.* differ from ours (see their Table I).

Although the comparisons in this section shed some light on the approximations made in the theoretical study, they are not definitive. Nor do they explain the large differences between the theoretical and experimental vibrational-excitation cross sections at energies around 1·0 eV. So we turn now to an error analysis of the swarm measurements and the unfolding of cross sections from transport data.

7.2 Swarm Experiments and Their Analysis

Before looking for possible sources of error in the experiments and their analysis we should note the extent to which the theoretical vibrational cross section appears to be incompatible with the results of swarm experiments. We say 'appears' because it is one of the purposes of this section to examine the significance of the mismatch.

In Fig. 18 the differences between measured transport coefficients and those calculated using theoretical cross sections for momentum-transfer and rotational and vibrational excitation are expressed as percentages of the experimental values and plotted as functions of E/N. We note first the excellent agreement below $E/N = 2$ Td, reflecting the agreement between theory and experiment for the momentum-transfer and rotational-excitation cross sections (cf. Section 2 and Fig. 4). However, for $E/N > 2$ Td, that is, in the range of E/N most sensitive to vibrational excitation, the calculated values lie up to five times outside the claimed experimental error limits (1% for v_{dr} and 2% for D_T/μ).

The comparisons of the vibrational cross sections shown in Fig. 7 throw doubt on the swarm result at energies between 0·7 and 1·5 eV, where the reliability of the beam experiment improves. On the other hand, the swarm experiment and analysis can *in principle* yield a definitive cross section at these energies provided the rotational cross section is known with reasonable accuracy (see Section 4.1)—and a great deal of attention has been paid to getting such a result. If this result is incorrect, what might have gone wrong?

To answer this question we look in detail at the procedure that is followed in determining a set of swarm-derived cross sections. The overall process has been summarised in Section 2 and Fig. 1. The steps leading up to a comparison of experimental and calculated transport coefficients are: measurements of the basic physical quantities to provide the primary data (step 1);derivations of drift velocities

and D_T/μ ratios from these data (step 2); and calculations of drift velocities and D_T/μ ratios from an assumed set of cross sections (step 3). Errors may occur in any of these steps, so we examine each of them in turn.

An example of the subtleties in step 2 has been given by Tagashira (1987) when discussing the interpretation of drift velocity experiments. In the present study this step is free of the problems he discussed since ionisation does not occur at the energies of interest. Nevertheless, additional subtleties remain in the interpretation of these experiments due to the effects of diffusion on the drifting electron groups. The interpretation of the lateral diffusion experiments from which the D_T/μ ratios are derived is more difficult. Both problems, however, have been dealt with at length (see Huxley and Crompton 1974 and references therein), so it is now possible to choose experimental conditions that allow the transport coefficients to be determined with minimum error, typically 1 or 2%.

Rather than introduce the intermediate step of inferring transport coefficients from the experimental measurements, then comparing them with values calculated theoretically for a given set of cross sections and experimental conditions, it would be preferable to have a complete theoretical description or simulation that would enable the quantities that are measured experimentally (e.g. current ratios in the Townsend–Huxley experiment—see e.g. Huxley and Crompton 1974) to be calculated directly. Such calculations would include the influence of the assumed boundary conditions (Kumar 1987). So far such a procedure has not been developed.

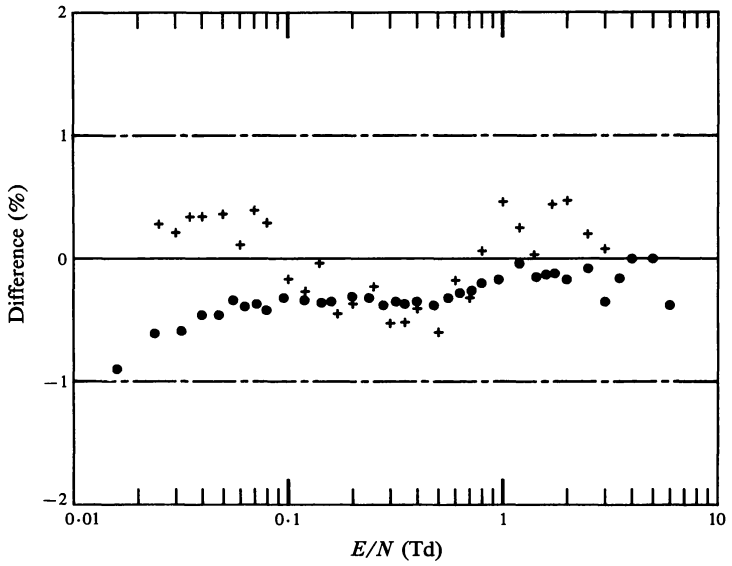

Fig. 19. Differences between the measured values of v_{dr} and D_T/μ in He and those calculated using Nesbet's (1979) theoretical cross section: circles, v_{dr}; crosses, D_T/μ.

The introduction of the intermediate step introduces errors that are difficult to estimate accurately. Nevertheless, there is evidence to suggest that the procedure currently in use is valid to the claimed accuracy when the experimental conditions are similar to those used for the hydrogen experiments. This evidence comes

from comparison of the transport coefficients determined from drift and diffusion experiments in helium (see Huxley and Crompton 1974) with values calculated using Nesbet's (1979) *ab initio* theoretical elastic momentum-transfer cross section for which an uncertainty of $\pm 1\%$ has been claimed. Percentage differences between experimental and calculated values of v_{dr} and D_T/μ in He are plotted in Fig. 19. For $E/N > 5\times10^{-2}$ Td the agreement suggests that the experimental error bounds are conservative; there is no reason to believe that the experiment is less accurate for lower values.

In moving from this example, which involves only elastic scattering, to e–H_2 scattering, the most suspect of the three steps summarised in Fig. 1 is the calculation of the transport coefficients from a set of cross sections. In recent years there has been much more debate about this step. Several theoretical analyses (Lin *et al.* 1979; Pitchford and Phelps 1982; McMahon 1983; Segur *et al.* 1983; Robson and Ness 1986) and computer simulations (personal communications from G. L. Braglia, H. R. Skullerud, and J. N. Bardsley) have examined the validity of the transport theory that was used at the time of the original analysis of the para-hydrogen transport data (Crompton *et al.* 1969, 1970). These studies showed that in certain circumstances (but not those pertaining to the para-hydrogen studies) transport coefficients calculated using theory based on the two-term approximation (see Section 2) were subject to errors much larger than those we are seeking. However, it is unlikely that the cause of the present discrepancy can be found here, for in our analysis we have used one of the new generation multi-term Boltzmann codes (Lin *et al.* 1979). The accuracy of this program has been checked as part of a comparison between a number of Boltzmann codes and computer simulations (see e.g. Segur *et al.* 1984, 1987). We also note the excellent agreement, in the region dominated by rotational excitation, between the measured transport coefficients and those calculated using the theoretical cross sections (see Fig. 6). This agreement cannot be explained on the grounds that rotational excitation exerts only a minor influence on the transport coefficients and therefore that this situation is similar to that for helium, because elimination of rotational excitation changes D_T/μ by 130% and v_{dr} by 45% (Crompton and Morrison 1987). We conclude, therefore, that if the origin of the disagreement between theory and experiment lies in the experiment or its interpretation, then an unsuspected source of error must arise when vibrational excitation becomes the important inelastic process.

8. Conclusion: Where do We go from Here?

The end-point of our work is an impasse that clearly requires resolution. We have attempted a thorough analysis of the possible sources of error in the present theoretical and experimental studies, seeking an explanation for the significant difference between the vibrational cross sections derived from each; this difference is particularly baffling given the excellent agreement for the momentum-transfer and rotational-excitation cross sections. An important facet of our work is that the disagreement *cannot* be ignored, since the interplay between theory and experiment, which has been a central feature of our work, has resulted in a significant reduction in the uncertainty assigned to the experimental result.

We make the following suggestions for future action. It is tempting to infer that the close agreement between theory and the experimental result of Ehrhardt *et al.*

(1968) for the vibrational-excitation cross section between about 0·7 and 1·5 eV implies that the swarm result must be incorrect in this energy range. Notwithstanding the support this agreement gives to both theory and this beam experiment, we note that determining a highly accurate absolute cross section in the threshold region was not the principal motivation for the experiments of Ehrhardt *et al.* (Ehrhardt, personal communication). Subsequent progress in measuring absolute cross sections at low energies by crossed-beam techniques, plus the present predicament, argues strongly for a new crossed-beam measurement of the cross section from threshold to a few eV with the highest possible accuracy. A further independent check of the swarm result—in addition to that of Haddad and Crompton (1980)—should also be made. A further set of experiments with this aim, using hydrogen–helium mixtures, is described in the companion paper (Petrović and Crompton 1987; present issue p. 347), and another experiment using hydrogen–neon mixtures is planned. Finally, an independent theoretical determination of the vibrational-excitation cross section should be undertaken. Only such a calculation can definitely resolve questions concerning the model potentials used in the present theoretical calculations.

We believe much rests on the resolution of this problem: either there is an obscure source of error in the theory that might prove even more serious when applied to more complex systems, or there is an unexpected flaw in the swarm experiments or their analysis that would limit their usefulness if it were to remain uncorrected.

Acknowledgments

The authors owe a considerable debt of gratitude to many colleagues who have participated in various aspects of this research: in the theoretical group, we wish to thank Drs Andrew N. Feldt and Thomas L. Gibson for their help with the design of the scattering codes and determination of the polarisation potentials, respectively, and David Austin and Rick Weitzel for assistance with endless calculations; in the swarm group, we wish to thank Dr Gerald Haddad for assistance with some of the calculations. We have also benefitted from extensive discussions of this work, notably with Prof. H. Ehrhardt and Drs David Norcross, Barry I. Schneider, Lee A. Collins, and Neal F. Lane. Finally, we are grateful to Dr Wolfgang Domcke for sending us tabulations of his results on e–H_2 scattering, and to Dr Malcolm Elford and Mr Daryl Boyd for their critical reading of the manuscript and their many helpful suggestions. The theoretical research reported here was supported by a grant from the National Science Foundation (PHY-8505438).

References

Arthurs, A. M., and Dalgarno, A. (1960). *Proc. R. Soc. London* A **256**, 540.
Bedersen, B., and Kieffer, L. J. (1971). *Rev. Mod. Phys.* **43**, 601.
Berman, M., Mündel, C., and Domcke, W. (1985). *Phys. Rev.* A **31**, 641.
Buckman, S. J., and Lohmann, B. (1986). *J. Phys.* B **19**, 2547.
Buckman, S. J., and Phelps, A. V. (1985). *J. Chem. Phys.* **82**, 4999.
Bulos, B. R., and Phelps, A. V. (1976). *Phys. Rev.* A **14**, 615.
Burke, P. G., Noble, C. J., and Salvini, S. (1983). *J. Phys.* B **16**, L113.
Castillejo, L., Percival, I. C., and Seaton, M. J. (1960). *Proc. R. Soc. London* A **254**, 259.
Chang, E. S., and Fano, U. (1972). *Phys. Rev.* A **6**, 173.
Chase, D. M. (1956). *Phys. Rev.* **104**, 838.
Collins, L. A., and Morrison, M. A. (1982). *Phys. Rev.* A **25**, 1764.

Collins, L. A., Robb, W. D., and Morrison, M. A. (1980). *Phys. Rev.* A **21**, 488.
Collins, L. A., and Schneider, B. I. (1981). *Phys. Rev.* A **24**, 2387.
Crompton, R. W. (1969). *Adv. Electron. Electron Phys.* **27**, 1.
Crompton, R. W. (1983). Proc. XVI Int. Conf. on Phenomena in Ionised Gases, Düsseldorf (Eds W. Bötticher *et al.*), p. 58 (Univ. of Düsseldorf).
Crompton, R. W., Elford, M. T., and Jory, R. L. (1967). *Aust. J. Phys.* **20**, 369.
Crompton, R. W., Gibson, D. K., and McIntosh, A. I. (1969). *Aust. J. Phys.* **22**, 715.
Crompton, R. W., Gibson, D. K., and Robertson, A. G. (1970). *Phys. Rev.* A **2**, 1386.
Crompton, R. W., and Morrison, M. A. (1987). *In* 'Swarm Studies and Inelastic Electron–Molecule Collisions' (Eds L. Pitchford *et al.*), p. 143 (Springer: New York).
Dalba, G., Fornasini, P., Lazzizzera, I., Ranieri, G., and Zecca, A. (1980). *J. Phys.* B **13**, 2839.
Ehrhardt, H., Langhans, L., Linder, F., and Taylor, H. S. (1968). *Phys. Rev.* **173**, 222.
Faisal, F. H. M., and Temkin, A. (1972). *Phys. Rev. Lett.* **28**, 203.
Ferch, J., Granitza, B., Masche, C., and Raith, W. (1985). *J. Phys.* B **18**, 967.
Ferch, J., Raith, W., and Schröder, K. (1980). *J. Phys.* B **13**, 1481.
Feshbach, H. (1958). *Ann. Phys. (New York)* **5**, 357.
Gibson, T. L., Lima, M. A. P., Takatsuka, K., and McKoy, V. (1984). *Phys. Rev.* A **30**, 3005.
Gibson, T. L., and Morrison, M. A. (1981). *J. Phys.* B **14**, 727.
Gibson, T. L., and Morrison, M. A. (1984). *Phys. Rev.* A **29**, 2497.
Golden, D. E., Bandel, H. W., and Salerno, J. A. (1966). *Phys. Rev.* **146**, 40.
Haddad, G. N., and Crompton, R. W. (1980). *Aust. J. Phys.* **33**, 975.
Haddad, G. N., and Elford, M. T. (1979). *J. Phys.* B **12**, L743.
Hara, S. (1967). *J. Phys. Soc. Jpn* **22**, 710.
Hara, S. (1969). *J. Phys. Soc. Jpn* **27**, 1592.
Henry, R. J. W., and Lane, N. F. (1969). *Phys. Rev.* **183**, 221.
Hoffman, K. R., Dababneh, M. S., Hsieh, Y.-F., Kauppila, W. E., Pol, V., Smart, J. H., and Stein, T. S. (1982). *Phys. Rev.* A **25**, 1393.
Huxley, L. G. H., and Crompton, R. W. (1974). 'The Diffusion and Drift of Electrons in Gases' (Wiley: New York).
Jones, R. K. (1985). *Phys. Rev.* A **31**, 2898.
Jung, K., Antoni, Th., Müller, R., Kochem, K.-H., and Ehrhardt, H. (1982). *J. Phys.* B **15**, 3535.
Kochem, K.-H., Sohn, W., Jung, K., Ehrhardt, H., and Chang, E. S. (1985). *J. Phys.* B **18**, 1253.
Kolos, W., and Wolniewicz, L. (1967). *J. Chem. Phys.* **46**, 1426.
Kumar, K. (1987). *In* 'Swarm Studies and Inelastic Electron–Molecule Collisions' (Eds L. Pitchford *et al.*), p. 63 (Springer: New York).
Kumar, K., Skullerud, H. R., and Robson, R. E. (1980). *Aust. J. Phys.* **33**, 343.
LaBahn, R. W., and Callaway, J. (1970). *Phys. Rev.* A **2**, 366.
Lane, N. F. (1980). *Rev. Mod. Phys.* **52**, 29.
Lane, N. F., and Henry, R. J. W. (1968). *Phys. Rev.* **173**, 183.
Lawton, S. A., and Phelps, A. V. (1978). *J. Chem. Phys.* **69**, 1055.
Lin, S. L., Robson, R. E., and Mason, E. A. (1979). *J. Chem. Phys.* **71**, 3483.
Linder, F., and Schmidt, H. (1971). *Z. Naturforsch.* **26a**, 1603.
Lucchese, R. R., Takatsuka, K., and McKoy, V. (1986). *Phys. Rep.* **131**, 147.
MacAdam, K. B., and Ramsey, N. F. (1972). *Phys. Rev.* A **6**, 898.
McMahon, D. R. A. (1983). *Aust. J. Phys.* **36**, 163.
Milloy, H. B., Crompton, R. W., Rees, J. A., and Robertson, A. G. (1977). *Aust. J. Phys.* **30**, 61.
Morrison, M. A. (1980). *Comput. Phys. Commun.* **21**, 63.
Morrison, M. A. (1983). *Aust. J. Phys.* **36**, 239.
Morrison, M. A. (1987). *Adv. Atom. Mol. Phys.* (in press).
Morrison, M. A., and Collins, L. A. (1978). *Phys. Rev.* A **17**, 918.
Morrison, M. A., and Collins, L. A. (1981). *Phys. Rev.* A **23**, 127.
Morrison, M. A., Feldt, A. N., and Austin, D. (1984*a*). *Phys. Rev.* A **29**, 2518.
Morrison, M. A., Feldt, A. N., and Saha, B. C. (1984*b*). *Phys. Rev.* A **30**, 2811.
Morrison, M. A., and Hay, P. J. (1979). *Phys. Rev.* A **20**, 740.
Morrison, M. A., and Lane, N. F. (1979). *Chem. Phys. Lett.* **66**, 527.
Morrison, M. A., and Saha, B. C. (1986). *Phys. Rev.* A **34**, 2786.
Nesbet, R. K. (1979). *Phys. Rev.* A **20**, 58.

Ness, K. F., and Robson, R. E. (1986). *Phys. Rev.* A **34**, 2185.
Newell, A. C., and Baird, R. C. (1965). *J. Appl. Phys.* **36**, 3751.
Petrović, Z. Lj., and Crompton, R. W. (1987). *Aust. J. Phys.* **40**, 347.
Pitchford, L. C., and Phelps, A. V. (1982). *Phys. Rev.* A **25**, 540.
Robson, R. E., and Ness, K. F. (1986). *Phys. Rev.* A **33**, 2068.
Rohr, K. (1977). *J. Phys.* B **10**, 2215.
Schmid, G. B., Norcross, D. W., and Collins, L. A. (1980). *Comput. Phys. Commun.* **21**, 79.
Schneider, B. I., and Collins, L. A. (1983). *Phys. Rev.* A **27**, 2847.
Schulz, G. J. (1973). *Rev. Mod. Phys.* **45**, 423.
Segur, P., Bordage, M. C., and Yousfi, M. (1987). *In* 'Swarm Studies and Inelastic Electron–Molecule Collisions' (Eds L. Pitchford *et al.*) (Springer: New York).
Segur, P., Bordage, M. C., Balageur, J. P., and Yousfi, M. (1983). *J. Comput. Phys.* **50**, 116.
Segur, P., Yousfi, M., and Bordage, M. C. (1984). *J. Phys.* D **17**, 2199.
Shugard, M., and Hazi, A. U. (1975). *Phys. Rev.* A **12**, 1895.
Tachibana, K., and Phelps, A. V. (1979). *J. Chem. Phys.* **71**, 3544.
Tagashira, H. (1981). Proc. Int. Conf. on Phenomena in Ionised Gases, Minsk, p. 377.
Tagashira, H. (1987). *In* 'Swarm Studies and Inelastic Electron–Molecule Collisions' (Eds L. Pitchford *et al.*), p. 55 (Springer: New York).
Temkin, A. (1957). *Phys. Rev.* **107**, 1004.
Trajmar, S., Register, D. F., and Chutjian, A. J. (1983). *Phys. Rep.* **97**, 219.
Wong, S. F., and Schulz, G. J. (1974). *Phys. Rev. Lett.* **32**, 1089.

Manuscript received 31 October 1986, accepted 5 February 1987